ARTICLE

doi:10.1038/nature24285

Disorder in convergent floral nanostructures enhances signalling to bees

Edwige Moyroud[1]*, Tobias Wenzel[2]*, Rox Middleton[3], Paula J. Rudall[4], Hannah Banks[4], Alison Reed[1], Greg Mellers[1], Patrick Killoran[1], M. Murphy Westwood[1], Ullrich Steiner[2,5], Silvia Vignolini[3] & Beverley J. Glover[1]

Diverse forms of nanoscale architecture generate structural colour and perform signalling functions within and between species. Structural colour is the result of the interference of light from approximately regular periodic structures; some structural disorder is, however, inevitable in biological organisms. Is this disorder functional and subject to evolutionary selection, or is it simply an unavoidable outcome of biological developmental processes? Here we show that disordered nanostructures enable flowers to produce visual signals that are salient to bees. These disordered nanostructures (identified in most major lineages of angiosperms) have distinct anatomies but convergent optical properties; they all produce angle-dependent scattered light, predominantly at short wavelengths (ultraviolet and blue). We manufactured artificial flowers with nanoscale structures that possessed tailored levels of disorder in order to investigate how foraging bumblebees respond to this optical effect. We conclude that floral nanostructures have evolved, on multiple independent occasions, an effective degree of relative spatial disorder that generates a photonic signature that is highly salient to insect pollinators.

A common mechanism that produces structural colour in living organisms is one-dimensional periodic nanostructuring on organ surfaces; examples of this are found in both the animal and plant kingdoms[1,2]. In a small number of flowering plant species, parallel striations of the cuticle on the petal epidermis have been approximated to diffraction gratings[2,3]. Petal cells with parallel cuticular striations contrast in form and function with smooth cuticular surfaces or with surfaces in which the cuticle of each epidermal cell has radiating striations. In *Hibiscus trionum*, the white region of the petal epidermis consists of smooth conical cells and the red pigmented region has flat cells with parallel striations; the latter generate a visible and measurable weak iridescent signal[2,3]. Foraging bumblebees can use the optical signals arising from ordered diffraction gratings and floral striations as cues to identify food sources. These floral signals increase the salience of the flower, without compromising search image formation[2,4].

Although parallel floral striations have some local order, they (like other natural structures[5]) are often appreciably disordered; the size and spacing of the striations on a single organ vary to a degree that would not occur in manmade grating structures. To investigate the evolutionary and functional significance of these disordered structures, we explored their distribution across the angiosperm phylogenetic tree and found convergent evolution[6] of similar parallel surface striations on differently pigmented flowers in most major lineages. Analysis of this uncommon but phylogenetically widespread floral trait indicates that, despite structural differences, these photonic structures have converged on a similar degree of disorder, which invariably generates a predominantly blue or ultraviolet (UV) scattering effect. We investigated the responses of foraging bumblebees to artificial surfaces that reproduce this angle-dependent blue–UV scattering and found that the effect is sufficient to allow pollinators to identify rewarding flowers and to enhance foraging efficiency. We interpret the degree of relative disorder in convergent floral photonic structures as an adaptive trait that generates strongly insect-salient optical signals.

Phylogenetic distribution of striations

The grating-like structures that generate a weak iridescent signal on *H. trionum* petals are formed from roughly parallel folds or striations of the cuticle on flat epidermal cells[1,2]. The infrequency of flat petal cells might in part explain the sparse distribution of grating-like structures in flowering plants. To analyse the distribution of this photonic structure in flowering plants, we surveyed the floral surfaces of species (selected from families representing the major angiosperm groups) with flat epidermal cells. We used scanning electron microscopy (SEM) to identify species with ordered cuticular striations on the pollinator-attracting (usually adaxial) surface of the petal, tepal or bract (the floral organ that is most attractive to insect pollinators). We identified ordered or quasi-ordered striations on the surfaces of flowers from almost all major branches of the angiosperm phylogeny[7], except the early-divergent lineages (Fig. 1). The striations on the bracts of *Trimenia moorei*, an Amborellaceae–Nymphaeales–Austrobaileyales (ANA)-grade early-divergent angiosperm that is probably wind pollinated[8], appeared insufficiently ordered to generate a large-scale optical signal (Fig. 1a). As no other species in the ANA grade was found to possess ordered parallel striations, we conclude that floral grating-like structures most probably arose after the divergence of the early-branching extant angiosperm lineages.

The early diversification of the major clades of monocots and eudicots (together comprising 95% of angiosperm species) during the Cretaceous period coincided with the early evolution of major groups of flower-visiting insects[9,10] (in particular, nectar-sucking bees with siphonate mouthparts)[11]. We identified several examples of ordered parallel ridges that generate a measurable angle-dependent colour signal among both monocots and eudicots (Figs 1b–l, 2 and Extended Data Figs 1–4). Among the monocots, two orders (Asparagales and Liliales) contain species that display highly ordered ridges on long tabular tepal cells (Fig. 1b, k). In the highly diverse eudicot clade, members of several groups possess parallel cuticular striations on their petals; for example,

[1]Department of Plant Sciences, University of Cambridge, Downing Street, Cambridge CB2 3EA, UK. [2]Department of Physics, University of Cambridge, JJ Thomson Avenue, Cambridge CB3 0HE, UK. [3]Department of Chemistry, University of Cambridge, Lensfield Road, Cambridge CB2 1EW, UK. [4]Royal Botanic Gardens, Kew, Richmond, Surrey TW9 3AB, UK. [5]Adolphe Merkle Institute, Chemin des Verdiers 4, CH1700 Fribourg, Switzerland.
*These authors contributed equally to this work.

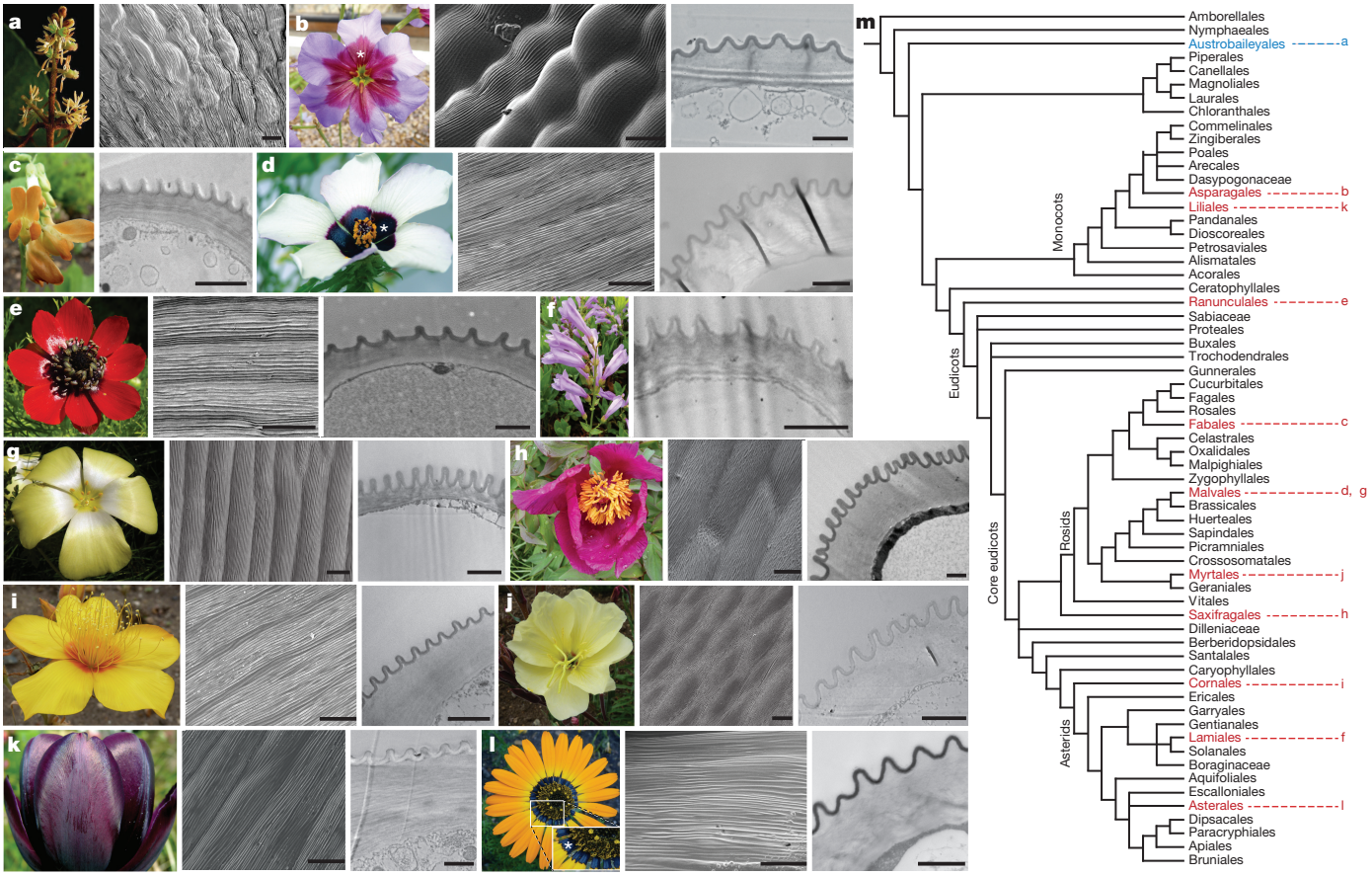

Figure 1 | Floral grating-like structures in angiosperms. Parallel cuticular striations on flat cells in the angiosperms *Trimenia moorei* (**a**), *Leucocoryne purpurea* (**b**), *Lathyrus aureus* (**c**), *H. trionum* (**d**), *Adonis aestivalis* (**e**), *Penstemon barrettiae* (**f**), *Grielum humifusum* (**g**), *Paeonia mascula* (**h**), *Mentzelia lindleyii* (**i**), *Oenothera stricta* (**j**), *Tulipa* 'Queen of the Night' (**k**) and *Ursinia speciosa* (**l**), none of which belong to the same angiosperm family (**m**). Iridescence was recorded in 11 taxa (red). *T. moorei* (blue) is the only early-diverging species in which we identified semi-ordered striations, but optical measurements were not performed on it. Left, flower. Middle (**b**, **d**, **e**, **g**–**l**) and right (**a**), SEM of abaxial (**c**, **f** and **k**) or adaxial (**a**, **b**, **d**, **e**, **g**, **h**, **i**, **j** and **l**) surface of the petal, tepal or bract. Proximal anthocyanin-rich region (**d** and **b**). Right (**b**–**l**), transmission electron microscopy (TEM) of transverse section of abaxial (**c**, **f** and **k**) or adaxial (**a**, **b**, **d**, **e**, **g**, **h**, **i**, **j** and **l**) epidermis. The striations cover the entire abaxial epidermis (**c**, **f** and **k**), entire adaxial epidermis (**a**, **e**, **g**, **h**, **i** and **j**) or are restricted to the central region (indicated by white asterisk) of the adaxial epidermis (**b**, **d** and **l**). Scale bars, 20 μm (right: **a**; middle: **b**, **d**, **e**, **g**–**l**), 2 μm (right: **b**–**l**).

in the early-divergent eudicot order Ranunculales, several species display striations (although most have smooth glossy surfaces)[12]. Among the rosids, parallel striations were found on petal surfaces of species of Fabales (Rosids I), Myrtales and Malvales (both Rosids II). Among the asterids, parallel striations are present in Cornales (an early-divergent clade), Lamiales (Asterids I) and Asterales (Asterids II); in this last group, some daisy species have parallel cuticular striations on their ray-floret petals (Fig. 1l). These flowers contain a range of pigments that present a variety of underlying colours. Although floral grating-like structures are relatively rare and flowers with angle-dependent colour have seldom been reported, this phylogenetically widespread distribution (Fig. 1m) suggests that parallel cuticular ridges have evolved iteratively in separate lineages, converging on an optically active signal in the flowers of distantly related groups.

Analysis of striated flower surfaces

Flower appearance is the result of the interplay between pigment content, epidermal cell shape[13,14] and photonic structures (if present)[15,16]. To better understand the structures that generate measurable angle-dependent flower colour, we analysed the parameters that characterize the striations in a range of angiosperm species. Fresh petals were collected from the species shown in Fig. 1 and their optical and anatomical properties were studied (Fig. 2, Extended Data Figs 1–4, and Extended Data Table 1). Figure 2 shows the scattering response, together with a characterization of the anatomical properties of the striations for three representative species that possess varying amounts of disorder. Although the flowers analysed have a range of pigment backgrounds (Fig. 1d, e, j), and striation heights, widths and spacing that are noticeably different from one another (Fig. 2a–c, Extended Data Figs 1–4 and Extended Data Table 1), all striations are formed from folds of the extracellular cuticle (Fig. 1). Notably, all the flowers that were analysed (Fig. 2a–c and Extended Data Figs 1–4) showed considerable disorder within a single petal in terms of the dimensions and spacing of their striations. The range of anatomical parameters, in combination with the disorder of the striations, suggests that the flowers of each species should possess distinct optical properties; our observations, however, contradict this.

To compare the effects of these disordered structures, we characterized their optical properties using an angle-resolved goniometer on a large area of the petal (3 mm in diameter). As the amount of disorder is an average property of the structure, the colour-dependent scattering in a petal must be measured over a large number of striations. Depending on the size of the illuminated area, the measurement of a semi-disordered surface may match the averages shown here or may appear randomly pixelated[17] (Extended Data Fig. 5). The scattering properties of the same area of the sample were measured in both the perpendicular and parallel planes with respect to the striation direction (Fig. 2d–i and Extended Data Figs 1–4). By comparing these two

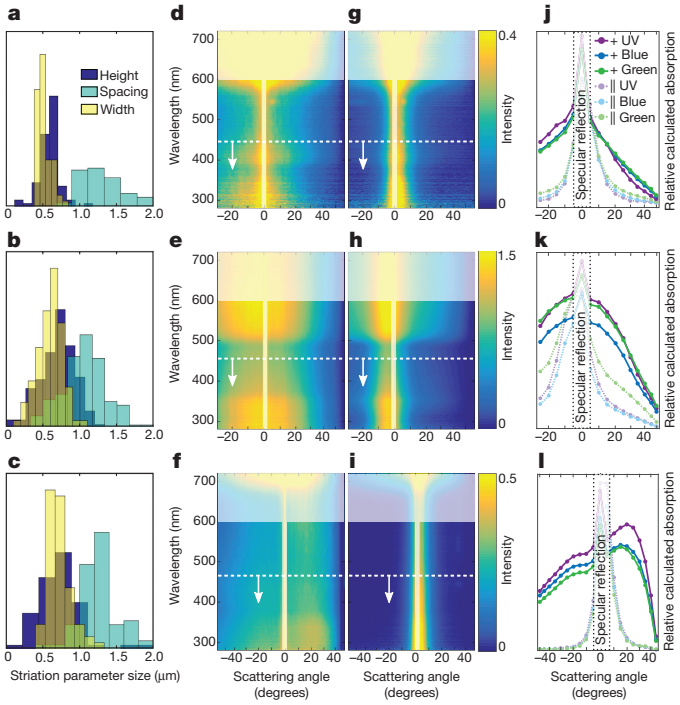

Figure 2 | Optical and anatomical properties of cuticular striations. The properties of three species: *A. aestivalis* (top), *O. stricta* (middle) and *H. trionum* (bottom). **a**–**c**, Distributions of striation height, spacing and width. **d**–**i**, Two-dimensional plots show spectra of scattered light at a range of collection angles, for a 30° (**d**, **e**, **g** and **h**) or 45° (**f** and **i**) angle of incident light. Light intensity is represented on a blue–yellow colour scale (constant within a single species but variable between species). Angular distribution of scattered light in the plane perpendicular (**d**–**f**) or parallel (**g**–**i**) to the striation direction is shown. The 600–700 nm spectral region (not perceived by bees) and the zero-order reflection are partially masked. Horizontal dotted lines with downward arrows indicate the enhanced spectral region of the blue halo. **j**–**l**, Angle-dependent spectral response averaged on the three photoreceptors in bee eyes: ultraviolet, blue and green. Spectra shown in the planes perpendicular (darker shades, + symbol) and parallel (lighter shades, || symbol) to the striation direction.

scattering responses, we analysed the contribution of three components to the overall optical signature of each flower: the effects of the pigment, the specular reflection (resulting from the air–petal interface) and the scattering attributable to the disordered petal striations. As all of these parameters vary for each species, we describe all the flowers in detail in the Supplementary Information and in Fig. 2d–i and Extended Data Figs 1–4. To highlight the visual effect of the disordered striation distribution on the petal surfaces, we compared the light scattered by the striations with its reference in three wavelength regions, corresponding to the spectral sensitivity of the three bee photoreceptors (Fig. 2j–l and Extended Data Figs 1–4; see methodology in Supplementary Information).

By comparing the scattering results and considering the role of pigments, we observed that the presence of the disordered striations contributes to the optical response of all the flowers in a similar way: the scattering response collected perpendicularly to the striations is enhanced in the blue–UV wavelength region, and is most intense between −25° and +25°. We term this directional scattering effect the 'blue halo'. The blue halo can be attributed to the presence of the striations, because it is present only in the measurement plane perpendicular to the striations. At higher wavelengths, the scattering effect is spread over a wider range of angles and is overridden by the dominant effect of the pigment (Extended Data Fig. 6 and Supplementary Discussion). Flowers showing a human-visible blue halo effect are shown in Extended Data Fig. 7a–d.

Modelling disorder and its optical signal

To further investigate the origin of the blue halo and to explore the design principles necessary to generate a bio-mimetic nanostructured surface capable of an angle-selective response for a specific wavelength interval[18], we approximated the petal epidermis to a disordered rectangular grating and studied it using finite-difference time-domain (FDTD) calculations. The purpose of this study was to investigate directional scattering caused by disordered gratings, and to compare this effect to the measurements obtained from the different flower species. In our approximation, the relatively low plant-cell surface curvatures were not considered because the scattering produced by disordered gratings is tolerant to surface curvature[19,20]; pigmentation, which adds an angle-independent background, was also omitted. Each striation was represented as a rectangular ridge with height, width and spacing parameters (Supplementary Methods). Figure 3 shows the spectral response predicted for rectangular gratings with varying degrees of disorder in ridge position and size. The results are an average of 60 disorder implementations, with 100 single ridges each (Extended Data Figs 5 and 8).

In the case of a perfectly ordered diffraction grating, in which the size of the ridges is kept constant and their spacing is perfectly periodic, the optical response exhibits the well-defined wavelength-dependent diffraction peaks characteristic of grating-derived iridescence (Fig. 3a). The introduction of less than 25% of the disorder observed in *H. trionum* flowers (Extended Data Fig. 8b, less than 10% relative Gaussian variation in height, and 6% variation in width and spacing, compared to a perfect grating) gives rise to angle-dependent scattering that is more intense in the blue–UV region than elsewhere in the spectrum, similar to the scattering in real flowers. As the amount of disorder increases up to the ratio present in *H. trionum* flowers, and further on to twice that value, the scattering intensity increases and the diffraction orders decrease (Fig. 3b, c and Extended Data Fig. 8).

Next, we calculated the spectral response for disorder values matching the parameters of the flowers in Fig. 1 (Fig. 3b, Extended Data Fig. 5 and Extended Data Table 1). In all cases, a blue halo was observed; this halo remained present at higher randomization values (typically twice the floral values, see Fig. 3c and Extended Data Fig. 8b, f). With increasing disorder, the intensity of the grating-like diffraction orders decreases, and disappears at approximately the level of disorder present in most of the flowers we studied (Fig. 3b and Extended Data Figs 5a–k, 8c).

From the FDTD calculation we observe that the blue halo is not strongly affected by the amount of disorder, across a wide range of striation spacing and shape parameters. This range of disorder encompasses the parameters extracted from all the flowers we investigated, indicating that the optical signals arising from their surface striations will be similar to one another (Extended Data Fig. 5a–k). The remaining differences between the photonic effects of the species we examined are primarily explained by their average striation spacing, which defines the width of the angular region into which most light is scattered. In flowers in which the regularity of striations is relatively high, the grating-like diffraction is partially retained (see measurement peaks at about 25° in Fig. 2f, l and Extended Data Figs 2d, i, 3b, f).

The results of the FDTD calculation were confirmed by experimental optical measurements from artificial surfaces produced with the same parameters as those used in the calculations (Fig. 3). Owing to manufacturing constraints, only two height levels were used (Extended Data Fig. 8g, h). A schematic of the fabrication steps and a cross-sectional SEM of the final structure are shown in Fig. 3d, e. The optical response of the artificial surface shows the blue halo and no contribution of diffraction orders (Fig. 3f).

Bumblebee response to the blue halo

The optical effect produced by ridged petal surfaces is visible to insect pollinators[1], but it is not known whether bumblebees perceive the blue halo rather than the weak iridescent signal. We used artificial stimuli to

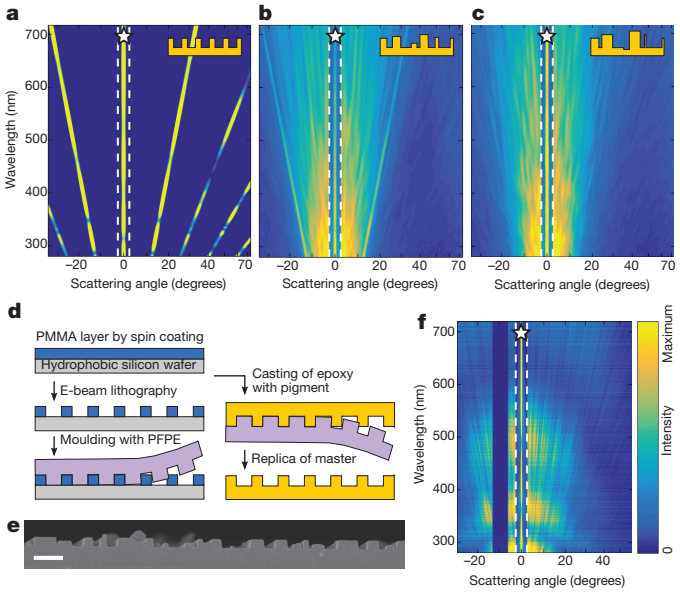

Figure 3 | Disorder in artificial striations. a, FDTD simulation results for rectangular ordered gratings with average parameters of *H. trionum* (730 nm height, 730 nm width, 1,300 nm spacing). **b**, As in **a**, but including disorder as found in *H. trionum* (standard deviations: 0.27 height, 0.16 width and 0.29 spacing). **c**, As in **b**, with twice the disorder of *H. trionum*. **d**, Schematic of manufacturing method. **e**, SEM image (2 μm scale bar) showing cross-section of an artificial disordered grating with two height levels. **f**, Optical goniometer reflectance measurement of a black artificial grating derived from *H. trionum* parameters, with twice the natural disorder in width and spacing and two height levels; the intensity of the reflected light is reported on a blue–white colour scale. Bands (stars) containing the zero-order reflections in **a**–**c** and **f** were reduced in intensity by a factor of three. Maximum colour scale values are 8×10^{-5} (normalized on incoming flux) for simulations (**a**–**c**) and 20 (normalized on white standard) for the optical measurement (**f**).

test this perception, because it was not possible to undertake pairwise comparisons of real flowers that were identical in all respects except for the presence of the blue halo. We used differential conditioning to test the ability of bumblebees (*Bombus terrestris*) to distinguish between pairs of stimuli that differed in terms of the presence of a blue halo, but were otherwise identical. Using the surfaces described above (Fig. 3d–f), we produced artificial flowers (Extended Data Fig. 7e–h) with a smooth surface; a manufactured, perfectly ordered (iridescent) grating; or a disordered (blue halo) grating (Fig. 4a). The spacing and width of the grating-like elements were chosen to match the average values of the *H. trionum* striations. For the perfectly ordered grating, these parameters were kept constant to generate strong iridescence and ensure no blue halo was present. For the disordered surfaces, the disorder in spacing and width of the elements was set at twice the disorder of *H. trionum* values to avoid any residual visible grating-like iridescence and produce only a blue halo. Artificial flowers were also coloured by adding one of several pigments to the epoxy, as all of the real flowers that were analysed had strong pigmentation underlying the blue halo. Regardless of the viewing angle, the colour of the smooth artificial flower matches the pigment, whereas the appearance of the manufactured striated surfaces varies (Fig. 4a).

We trained bumblebees using black smooth artificial flowers that contained a quinine hemisulfate salt solution (punishment) and identically pigmented artificial flowers producing a blue halo that offered a sucrose solution (reward), or vice versa (Fig. 4b). Bees were unable to distinguish rewarding flowers from punishing ones on the basis of cues derived directly from the quinine hemisulfate salt or sucrose solutions (Extended Data Fig. 9a, b). Over the course of the experiment, an increasing frequency of visits to flowers offering sucrose solution indicated that individual bees had learned to use the presence of the blue halo to discriminate between rewarding and punishing flowers. After 120 visits, bumblebees visited blue-halo flowers almost exclusively (mean of the final 10 visits: 8.9 ± 0.3), after showing no initial preference (mean of the first 10 visits: 4.9 ± 0.2) (Fig. 4b and Extended Data Fig. 9c). A fitted binomial logistic model of learning provided a significantly better fit than a null model ($\chi^2 = 104.64$, d.f. $= 1$, $P < 0.001$). Thus, experienced foragers are more likely to choose rewarding flowers than are naive foragers; they can see the blue halo on a dark pigmented background, and use it to identify rewarding flowers even when grating-like iridescence is absent. We repeated the experiment with black artificial flowers with a perfect diffraction grating in place of the blue-halo flowers (Fig. 4c and Extended Data Fig. 9d). After 120 visits, bumblebees visited the iridescent flowers more frequently than they had done initially, and had learned to identify rewarding flowers accurately ($\chi^2 = 100.30$, d.f. $= 1$, $P < 0.001$). However, by comparison with blue-halo flowers, learning appeared delayed (Extended Data Fig. 9, compare c to d). This could reflect the changeability of the signal: by producing a more consistent signal, natural disorder could facilitate search image formation.

In flowers with dark pigments, the blue halo effect is clearly visible to the human eye[2] (Extended Data Fig. 7a–d); by contrast, the blue halo is barely visible in flowers that possess pigments that appear light to us (for example, most flowers in Fig. 1). Artificial flowers with a disordered grating and a yellow pigment are consistently difficult for humans to distinguish from smooth yellow flowers (Extended Data Fig. 7f, compare with Fig. 4a). Compared with humans, however, bees have enhanced photoreceptor activity in the blue–UV parts of the spectrum. To explore the ability of bumblebees to perceive the blue halo on a yellow background, we repeated the differential conditioning using yellow flowers with a smooth surface or with a disordered grating (Fig. 4d and Extended Data Fig. 7f). Bumblebees initially showed no preference for one flower type over the other (mean of the first 10 visits: 5.4 ± 0.4, Extended Data Fig. 9e), but after 80 visits the bees almost always avoided flowers that contained quinine hemisulfate solution (mean of the final 10 visits: 9.4 ± 0.2, Extended Data Fig. 9e). As with dark pigmented backgrounds, a fitted binomial logistic model of learning provided a significantly better fit than a null model ($\chi^2 = 57.40$, d.f. $= 1$, $P < 0.001$, Fig. 4d). Bumblebees can also perceive the blue halo effect when it is associated with a blue background ($\chi^2 = 72.41$, d.f. $= 1$, $P < 0.001$, Fig. 4e and Extended Data Figs 7, 9f). We conclude that the blue halo is clearly visible to bumblebees even when associated with a yellow or blue pigmented background. We also note that the interaction between flowers and the environment is highly dynamic. As Extended Data Fig. 7a–d shows, the blue halo effect is particularly visible in full sun; this signal also probably takes on a different appearance in a moving flower in natural light than it does in the static replicas in our flight arena.

Floral structural colours have been shown to increase flower detectability[3]. To determine whether the blue halo alone is sufficient to influence bumblebee foraging efficiency, we measured the foraging speed of individuals on each flower type, using the artificial flowers depicted in Extended Data Fig. 7g[21]. We found that foraging speed varied significantly between the seven types of artificial flower analysed ($F_{6,65} = 13.9$, $P = 4.26 \times 10^{-10}$, Fig. 4f). The presence of the blue halo reduced travelling time ($F_{1,60} = 33.31$, $P = 2.95 \times 10^{-7}$). Bumblebees found black and yellow flowers with a blue halo more quickly than they found similarly pigmented smooth flowers (Tukey's honest significant difference (HSD) between black 'blue halo' and black 'smooth', or between yellow 'blue halo' and yellow 'smooth', $P < 0.0008$, Fig. 4f). Bumblebees performed equally well on black artificial flowers associated with a diffraction grating, regardless of the amount of disorder (Tukey's HSD between black 'blue halo' and black 'iridescent', $P = 0.96$, Fig. 4f). When associated with a blue pigment, the presence of a blue halo did not significantly improve foragers' efficiency (Tukey's HSD between blue 'blue halo' and blue 'smooth', $P = 0.40$, Fig. 4f). This

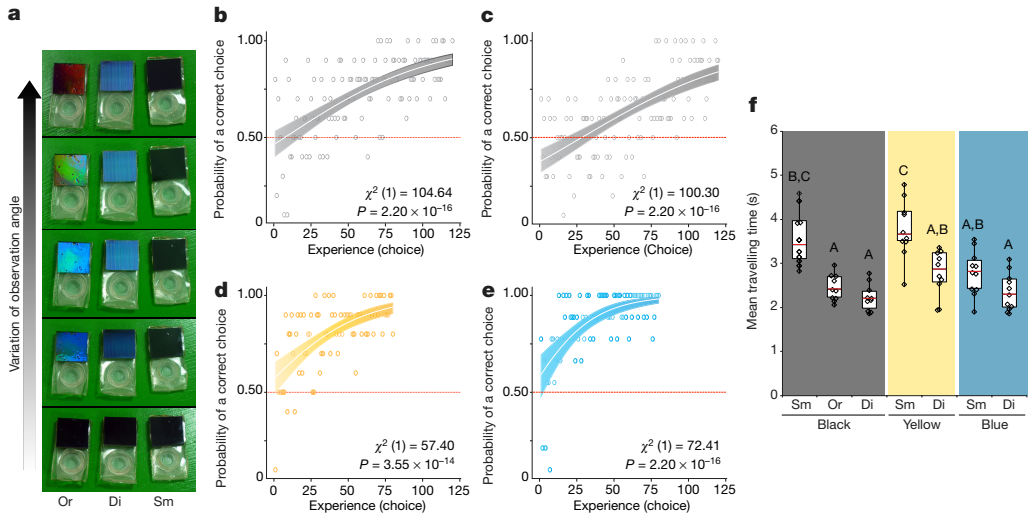

Figure 4 | Bumblebee responses to the blue halo. a, Angle-dependent appearance of black-pigmented artificial flowers with a smooth surface (Sm), or disordered (Di) or regular (Or) striations. **b**, Learning curve of ten bees choosing between artificial flowers with black smooth or disordered grating surfaces. Empty circles, mean proportion of bees choosing correctly for 120 successive choices. White curve, fitted binomial logistic model; grey shading, 95% confidence intervals on the fitted response. The χ^2 statistic (the number in brackets indicates d.f.) and *P* value for the likelihood ratio test (assessing whether foragers can learn) are given. **c**, As in **b**, but bumblebees chose between artificial flowers with black smooth or ordered grating surfaces. **d**, As in **b**, but bumblebees chose between artificial flowers with yellow smooth or disordered grating surfaces. **e**, As in **b**, but 11 bumblebees chose between artificial flowers with blue smooth or disordered grating surfaces. **f**, Distribution of the individual mean travel time between artificial flowers for seven pigment and surface combinations. Median flight time (red line), quartile values (boxes) and total range of flight times are represented. Diamonds, mean foraging times of individuals. A, B, C, results of a post hoc Tukey's HSD test. Group means that share the same letter are not significantly different from one another ($P > 0.001$).

suggests that, although the blue halo is visible on a blue background, the limited contrast between blue-pigmented flowers with or without blue haloes decreases the effect of the halo on salience. Interestingly, the foraging speeds the bees achieved on yellow and black flowers with a blue halo were similar to those recorded for blue-pigmented flowers (Tukey's HSD, $P > 0.16$ in all cases). Thus, disordered gratings could increase flower salience by giving the flower a blue appearance, even when blue pigments are absent. Previous researchers[3] have reported that bumblebees find red disks with a floral grating as quickly as they find smooth blue disks: our results suggest that this could be because the floral grating, unlike perfectly regular gratings, produces a blue halo that makes red disks appear 'bluer'.

Multiple wild species of bees have an innate preference for blue[22,23], which has been linked to the observation that flowers in the violet–blue range often produce relatively high volumes of nectar[24,25]. However, blue colour in petals is notoriously difficult to achieve[24–30]. Flowers use sophisticated mechanisms to produce blue signals, by increasing the pH of their vacuole or by creating metal–pigment complexes that blue-shift the appearance of anthocyanin[26–32]. Most angiosperms lack the genetic and biochemical capability to manipulate pigment chemistry in these ways and the presence of a disordered photonic structure on their petals could provide an alternative way to produce blue signals.

Conclusions

We conclude that disordered cuticular structures can generate biologically important colouration in flowers. Nanostructures with varying degrees of disorder appear to have evolved independently in the flowers of species in the major branches of the angiosperm phylogenetic tree; these structures converge on an overall disorder signature that consistently produces a directional scattering effect (the blue halo) in the UV–blue wavelength region of the spectrum, in addition to varying degrees of weak grating-like iridescence. As the blue halo alone can enhance bee foraging efficiency, and as UV–blue is an expensive and difficult colour to produce using conventional pigments, we conclude that these floral nanostructures have converged on an optimized form that generates signals that are salient to insect pollinators.

Online Content Methods, along with any additional Extended Data display items and Source Data, are available in the online version of the paper; references unique to these sections appear only in the online paper.

Received 12 January; accepted 19 September 2017.
Published online 18 October 2017.

1. Vukusic, P. & Sambles, J. R. Photonic structures in biology. *Nature* **424,** 842–845 (2003).
2. Whitney, H. M. *et al.* Floral iridescence, produced by diffractive optics, acts as a cue for animal pollinators. *Science* **323,** 130–133 (2009).
3. Vignolini, S. *et al.* The flower of *Hibiscus trionum* is both visibly and measurably iridescent. *New Phytol.* **205,** 97–101 (2015).
4. Whitney, H. M., Reed, A., Rands, S. A., Chittka, L. & Glover, B. J. Flower iridescence increases object detection in the insect visual system without compromising object identity. *Curr. Biol.* **26,** 802–808 (2016).
5. Prum, R. O. & Torres, R. H. A Fourier tool for the analysis of coherent light scattering by bio-optical nanostructures. *Integr. Comp. Biol.* **43,** 591–602 (2003).
6. Scotland, R. W. What is parallelism? *Evol. Dev.* **13,** 214–227 (2011).
7. The Angiosperm Phylogeny Group III. An update of the Angiosperm Phylogeny Group Classification for the orders and families of flowering plants: APG III. *Bot. J. Linn. Soc.* **161,** 105–121 (2009).
8. Endress, P. K. The evolution of floral biology in basal angiosperms. *Phil. Trans. R. Soc. Lond. B* **365,** 411–421 (2010).
9. Grimaldi, D. The co-radiations of pollinating insects and angiosperms in the Cretaceous. *Ann. Mo. Bot. Gard.* **86,** 373–406 (1999).
10. Grimaldi, D. & Engel, M. S. *Evolution of the Insects* (Cambridge Univ. Press, 2005).
11. Labandeira, C. C. The pollination of Mid Mesozoic seed plants and the early history of long-proboscid insects. *Ann. Mo. Bot. Gard.* **97,** 469–513 (2010).
12. Vignolini, S. *et al.* Directional scattering from the glossy flower of *Ranunculus*: how the buttercup lights up your chin. *J. R. Soc. Interface* **9,** 1295–1301 (2012).
13. Noda, K., Glover, B. J., Linstead, P. & Martin, C. Flower colour intensity depends on specialized cell shape controlled by a Myb-related transcription factor. *Nature* **369,** 661–664 (1994).
14. Gorton, H. L. & Vogelmann, T. C. Effects of epidermal cell shape and pigmentation on optical properties of antirrhinum petals at visible and ultraviolet wavelengths. *Plant Physiol.* **112,** 879–888 (1996).
15. Vignolini, S. *et al.* The mirror crack'd: both pigment and structure contribute to the glossy blue appearance of the mirror orchid, *Ophrys speculum*. *New Phytol.* **196,** 1038–1047 (2012).
16. van der Kooi, C. J., Elzenga, J. T. M., Staal, M. & Stavenga, D. G. How to colour a flower: on the optical principles of flower coloration. *Proc. R. Soc. Lond. B* **283,** 20160429 (2016).
17. van der Kooi, C. J. *et al.* Iridescent flowers? Contribution of surface structures to optical signaling. *New Phytol.* **203,** 667–673 (2014).

18. Johansen, V. E. *et al.* Designing visual appearance using a structured surface. *Optica* **2,** 239–245 (2015).
19. Schauer, S., Worgull, M. & Hölscher, H. Bio-inspired hierarchical micro- and nano-wrinkles obtained via mechanically directed self-assembly on shape-memory polymers. *Soft Matter* **13,** 4328–4334 (2017).
20. Schneider, N. *et al.* Nanothermoforming of hierarchical optical components utilizing shape memory polymers as active molds. *Opt. Mater. Express* **4,** 1895–1902 (2014).
21. Spaethe, J., Tautz, J. & Chittka, L. Visual constraints in foraging bumblebees: flower size and color affect search time and flight behavior. *Proc. Natl Acad. Sci. USA* **98,** 3898–3903 (2001).
22. Giurfa, M., Nunez, J., Chittka, L. & Menzel, R. Colour preferences of flower-naive honeybees. *J. Comp. Physiol. A* **177,** 247–259 (1995).
23. Raine, N. E., Ings, T. C., Dornhaus, A., Saleh, N. & Chittka, L. Adaptation, genetic drift, pleiotropy, and history in the evolution of bee foraging behavior. *Adv. Stud. Behav.* **36,** 305–354 (2006).
24. Raine, N. E. & Chittka, L. Nectar production rates of 75 bumblebee-visited flower species in a German flora (Hymenoptera: Apidae: *Bombus terrestris*). *Entomol. Gen.* **30,** 191–192 (2007).
25. Raine, N. E. & Chittka, L. The adaptive significance of sensory bias in a foraging context: floral colour preferences in the bumblebee *Bombus terrestris*. *PLoS One* **2,** e556 (2007).
26. Yoshida, K., Kondo, T., Okazaki, Y. & Katou, K. Cause of blue petal colour. *Nature* **373,** 291 (1995).
27. Yoshida, K., Mori, M. & Kondo, T. Blue flower color development by anthocyanins: from chemical structure to cell physiology. *Nat. Prod. Rep.* **26,** 884–915 (2009).
28. Holton, T. A. & Tanaka, Y. Blue roses — a pigment of our imagination? *Trends Biotechnol.* **12,** 40–42 (1994).
29. Hondo, T. *et al.* Structural basis of blue-colour development in flower petals from *Commelina communis*. *Nature* **358,** 515–518 (1992).
30. Katsumoto, Y. *et al.* Engineering of the rose flavonoid biosynthetic pathway successfully generated blue-hued flowers accumulating delphinidin. *Plant Cell Physiol.* **48,** 1589–1600 (2007).
31. Shiono, M., Matsugaki, N. & Takeda, K. Phytochemistry: structure of the blue cornflower pigment. *Nature* **436,** 791 (2005).
32. Sasaki, N. & Nakayama, T. Achievements and perspectives in biochemistry concerning anthocyanin modification for blue flower coloration. *Plant Cell Physiol.* **56,** 28–40 (2015).

Supplementary Information is available in the online version of the paper.

Acknowledgements We thank M. Dorling for plant and bee care; P. Cunha for advice on e-beam lithography; and B. Wilts, J. Baumberg, R. Bateman, N. Cunniffe, N. Walker-Hale, L. Chittka, H. Whitney and M. Kolle for discussion. We acknowledge the collections at Cambridge University Botanic Garden and the Royal Botanic Gardens, Kew. This work was funded by the Leverhulme Trust (F/09741/G to B.J.G. and U.S.), BBSRC (DTG studentship to A.R. and the David Phillips fellowship (BB/K014617/1) (76933) to S.V.), the European Research Council ((ERC-2014-STG H2020 639088) to S.V.), the Herchel Smith fund (to E.M.), EU Marie Curie actions (NanoPetals to E.M. and B.J.G.), EPSRC (EP/G037221/1 to R.M.), the Winton Fund for the Physics of Sustainability and the Cambridge Trust CHESS (to T.W.), the Adolphe Merkle Foundation and the Swiss National Science Foundation (National Center of Competence in Research Bio-Inspired Materials) (U.S.). We thank the EU for funding under Marie Curie Actions I.T.N. PlaMatSu (722842) to U.S., S.V. and B.J.G.

Author Contributions B.J.G., S.V., U.S., P.J.R. and E.M. conceived and led the project. B.J.G., S.V., U.S., E.M. and T.W. designed experiments. E.M., S.V., A.R. and M.M.W. surveyed collections and performed SEM imaging. E.M., H.B. and G.M. performed TEM imaging. S.V., R.M. and T.W. performed optical measurements. T.W. extracted striation parameters, ran finite-difference time-domain simulations, manufactured artificial gratings and conducted cross-sectional SEM. E.M. and P.K. performed bee behavioural experiments. B.J.G., E.M., T.W., S.V., U.S. and P.J.R. wrote the manuscript. All authors commented before submission.

Author Information Reprints and permissions information is available at www.nature.com/reprints. The authors declare no competing financial interests. Readers are welcome to comment on the online version of the paper. Publisher's note: Springer Nature remains neutral with regard to jurisdictional claims in published maps and institutional affiliations. Correspondence and requests for materials should be addressed to S.V. (sv319@cam.ac.uk) or B.J.G. (bjg26@cam.ac.uk).

Reviewer Information *Nature* thanks D. Deheyn and the other anonymous reviewer(s) for their contribution to the peer review of this work.

METHODS

No statistical methods were used to predetermine sample size. The experiments were not randomized, except where indicated otherwise. Investigators were not blinded to allocation during experiments and outcome assessment.

Scanning electron microscopy. For SEM, dissected petals were dehydrated through an ethanol series, critical point dried, mounted on metal stubs, and sputter-coated in platinum. The coated specimens were viewed using a Hitachi FE-SEM S-4700 scanning electron microscope. For cryo-SEM examination, the samples were imaged using a Hitachi S-4700 Cryo-SEM. For each sample, about 10 mm^2 of tissue was mounted on a stage, fixed by cooling in nitrogen slush, sputter-coated with gold in the antechamber of the SEM and introduced into the main chamber to be imaged.

Transmission electron microscopy. For TEM, samples were taken from between 4 and 11 flowers from at least 3 individual plants (or 2 plants for *L. purpurea*), over several years (June 2010–July 2016). For each sample, a 2 mm^2 region of petal tissue was dissected using a mounted needle, fixed in 2.5% glutaraldehyde in phosphate buffer at pH 7.4, and stored in 70% ethanol until needed. Samples were stained in 1% osmium tetroxide solution and passed through an ethanol and resin series before being polymerized for 18 h under vacuum. Semi-thin sections (0.5–2 μm) and ultra-thin sections (50−90 nm) were cut using a Jung Ultracut microtome. The semi-thin sections were mounted on glass slides and stained with toluidine blue in phosphate buffer, before being examined under a light microscope. The ultra-thin sections were placed on copper mesh grids before being examined using a Hitachi H-7650 transmission electron microscope.

Optical goniometer measurements. Reflection spectra were measured using an angular resolved setup. The light from an Ocean Optics HPX 2000 xenon source (wavelength range from −185 to 2,000 nm) passed through an optical fibre (Avantes 50 μm diameter) and a collimator (Thorlabs RC08SMA-F01), and was incident on the sample in a spot of 3–5 mm diameter, depending on the available sample size and angle. The illumination angle ranged from 5° to 60° with respect to the surface normal, and passed 0.3 m from source to sample and 0.22 m from sample to the collimator on the outlet optical fibre (Avantes 600 μm diameter). The reflected light was collected over a range of 100° and analysed with an Avantes (Avaspec 2048) spectrometer. As the optical goniometer provides access to scattered light in one dimension only, it is crucial to identify the direction of the striations on the petal before performing the measurement. This was achieved using a standard optical microscope; the direction of the striations on the petal (already fixed to the sample holder) were visualized using a 20× or 50× objective. Once the direction of the striations was determined, the sample holder was mounted in position in one of two configurations: (i) striations perpendicular to the plane in which the detector is rotated or (ii) striations parallel to the plane in which the detector is rotated. Although the optical response for the same flowers is comparable in each of the two configurations, when a range of species are used the response differs according to petal composition.

Spectral analysis with bee-eye sensitivity weighting. To clearly explain the effect of the striations on the scattering response of the flowers, we applied the following processing to the goniometer data. The scattering effect is dependent on wavelength; it is therefore necessary to consider the scattering in multiple spectral regions. We considered the spectral sensitivities associated with bee photoreceptors to be relevant spectral regions. The spectrum recorded by the goniometer at each angle was multiplied with the sensitivity curve of each of the three bee photoreceptors, referred to here as ultraviolet (in violet), blue (in blue), and green (in green) (Figs 2–4 and Extended Data Fig. 6). These weighted spectra were integrated over all wavelengths to yield one value per bee photoreceptor at each angle. These new angle curves were averaged in five-degree steps to simplify the data representation for the observer.

The photosensitivity curves for the bee photoreceptors were normalized to their integral before the multiplication. This normalization is necessary in our analysis. Other normalizations (such as normalizing to the peak value of each curve) would produce an unwanted bias when integrating over the weighted spectrum. This is due to the photoreceptors having distinct spectral shapes; the integral with the varying sensitivity curves would produce a range of integral factors.

It should also be noted that the bee photoreceptor that peaks in the wavelength range corresponding to green light is also sensitive to light in the blue and UV region of the spectrum; an increased signal in the UV will therefore also stimulate the green receptor, leading to an increased signal in the green curve. The spectra in the planes perpendicular and parallel to the striation direction are reported as darker and lighter colours respectively. See Supplementary Methods for a visual explanation.

Extraction of striation parameters. The mean and standard deviation of the striation parameters (height, width and spacing) were extracted for each flower from multiple cross-sectional TEM images. The outer striation edges were detected in Matlab. Non-striation edges were removed manually. The undulation caused by the shape of underlying cells was removed using a low-order polynomial fit. Pixels of consecutive striation edges were sorted, scaled and noise filtered, before local extrema were detected with the Matlab peakdet function (http://www.billauer.co.il/peakdet.html). Each striation element was resampled with the algorithm interparc (https://uk.mathworks.com/matlabcentral/fileexchange/34874-interparc?requestedDomain=www.mathworks.com) and the width was determined by averaging the position of the middle-third of the striation height. Further geometrical details of the striation parameters are shown in Supplementary Information.

Finite-difference time-domain simulations. In Lumerical software, a dielectric grating with a wavelength-independent refractive index of 1.5 was created, spanning 100 grating elements and non-periodic boundary conditions. A Gaussian light source was set up to illuminate the area such that the intensity was close to zero near the ends of the grating. A virtual monitor captured the reflected near-field and inferred the far-field response of the structure. Randomness was introduced to grating elements using random values with a Gaussian distribution, which were derived from the standard deviation from pre-determined floral values and truncated at twice the standard deviation. The spacing disorder was modelled by offsets around a fixed lattice (see Supplementary Methods). The presented simulation data are an average derived from over 60 implementations of disorder for each parameter set, ensuring a representative scattering distribution. Each individual simulation result represents an illuminated area of only approximately 0.1 mm; at this scale, the introduced randomness would lead to a pixelated appearance mainly determined by chance (see Extended Data Fig. 5l–s). Sixty implementations produced an illuminated length equivalent to about 6 mm, and yielded more realistic values. The alternative strategy of simulating a larger area with, for example, 6,000 grating elements in one simulation would lead to false assumptions because of the large coherence length: the light source in the presented simulations is perfectly coherent and would lead to interference from similar striation elements that are far apart, making the structure look more ordered than it would appear under sunlight illumination. In order to ensure comparability, the disorder parameters were seeded so that they varied between iterations of the same simulation but not between simulations of each of the statistical parameters of the grating disorder.

Artificial striations manufacturing process. Clean silicon wafer pieces were coated with a UNISOL adhesion layer. A PMMA film was spin-coated from PMMA 950 A9 solution with 15% (volume) of additional anisole solvent content. The spun PMMA films were annealed on a hotplate at 100 °C for 15 min. The patterns were created with an e-beam lithography system at 50 kV at currents between 2 and 5 nA, with a resolution of 30 nm. The spacing and width of grating elements were randomly varied around a fixed lattice (similar to the FDTD simulations) at twice the floral standard deviation, and the height constraint was relaxed by introducing one intermediate level. The height variation was enabled by dosage variation of the e-beam lithography process and precision development with a mixture of seven parts isopropyl alcohol and three parts deionized water[33]. The PMMA on the silicon master structure was moulded into a perfluoropolymer[34] in a nitrogen flow-through chamber with UV curing at 365 nm. Epoxy casts were created from the moulds using EPO-TEK optical epoxy (301-1LB kit) with the addition of pigments. The perfectly ordered gratings were produced in the same way as the controlled disordered striations; omitting the e-beam patterning step yielded flat reference samples.

Artificial flower design. Artificial flowers used in differential conditioning experiments were constructed from black microcentrifuge tubes (10 mm diameter, 1.5 ml volume) around which were mounted 20 mm × 40 mm strips of 3-mm-thick transparent Devcon high-strength 2-ton epoxy resin. Epoxy 'test-squares' (20 mm × 20 mm) containing black (carbon black) or yellow (Naples yellow light (PY41)) pigment (62.5 mg ml^{-1} epoxy) were added to the top of the transparent strips to act as a stimulus. The surface of the epoxy square was smooth and glossy, or overlain by a manufactured disordered or ordered grating (see above). These artificial flowers were mounted on 12-cm-long wooden skewers and oriented so that their surface was 35° from vertical, facing upward: the lid of the microcentrifuge tube was left attached and open to act as a feeding reservoir for foraging bees (see Extended Data Fig. 7e).

Artificial flowers used in foraging speed experiments had a modified design: the detached lid of a transparent microcentrifuge tube (10 mm in diameter), acting as a feeding device for foragers, was inserted in a 20 mm × 40 mm strip of 3-mm-thick transparent epoxy resin and a 20 mm × 20 mm epoxy test-square containing a black (carbon black), yellow (Naples yellow light) or blue (Ultramarine blue) pigment (62.5 mg ml^{-1} epoxy) was added to the top of the transparent strip to act as a stimulus. As in differential conditioning experiments, the surface of the epoxy square was smooth and glossy, or overlain by a manufactured disordered or ordered grating; in this case, though, the artificial flowers were laid flat directly on the floor of the arena (Extended Data Fig. 7g).

Bumblebee experiments. Flower-naive colonies of buff-tailed bumblebees, *B. terrestris* (*audax*), 'Research Hive, 1 Week Early' (Biobest UK), were connected

to test arenas ($100 \times 70 \times 30\,cm^3$) by a gated transparent perspex tube (15 mm diameter, 30 cm long) as described[1]. For each experiment, foragers from three colonies were used. The room temperature was kept constant at 21 °C. Illumination was provided for fourteen hours a day using Sylvania 36W Professional Activa 172 tubes on the ceiling of the room. The frequency of these lights was kept at over 200 Hz (above the bee-flicker fusion frequency) using Philips HF-B 236 TLD ballasts[35]. Adjustable lamps with a frequency of over 200 Hz, fitted with daylight bulbs, were placed above the colony entrance to control flower illumination. The colony was fed with fresh 30% sucrose solution daily and pollen grains were supplied three times a week. Foragers were hand-marked with water-based Thorne queen marking paint in various colour combinations to distinguish individuals during experimentation.

Differential conditioning experiments. During the training phase, each individual was allowed to familiarize itself with the feeding set-up. Three training flowers (as described above, but without any test-squares, see Extended Data Fig. 7e) containing 30 µl of 30% sucrose solution were randomly positioned in the arena; an individual bee was introduced into the arena and allowed to feed until it returned to the hive. A bee was considered trained after it had completed three successful bouts of foraging.

During the test phase, six differential conditioning artificial flowers (as described above) were randomly positioned in the arena. Three flowers presented a pigmented smooth test-square with 15 µl of 0.12% quinine solution and three flowers displayed a similarly pigmented test-square overlain by a manufactured grating paired with 15 µl of 30% sucrose solution (or vice versa). An individual trained bee was released into the arena, and the flowers that it successively visited were recorded. A flower was considered to have been visited whenever a bee made contact with it. After each visit, the flower was refilled with sucrose or quinine solution and moved to a new position in the arena; the positions of the non-visited flowers were also randomized. Consequently, the position of the six flowers changed constantly throughout the experiment. Parts of the flowers with which the bees came into contact were cleaned with 20% ethanol solution between each foraging bout and between individual bees (to remove scent marks). For each pairwise comparison (black smooth versus black blue halo; black smooth versus black iridescent; yellow smooth versus yellow blue halo; blue smooth versus blue 'blue halo'), ten bees were tested, except for the comparison between blue smooth and blue 'blue halo' artificial flowers, for which 11 bees were recorded (41 bees in total). Each bee was tested for up to a minimum of 120 choices (on black pigmented flowers) or 80 choices (yellow or blue pigmented flowers).

Insect learning curves associated with each pairwise comparison were obtained by pooling data from all individual bees. Preparatory analyses showed no pronounced differences between individual foragers within treatment groups, so we analysed the learning curve data in RStudio (Version 0.99.902) using binomial logistic regression[36,37] by fitting the fixed effect model (presented in Supplementary Methods) to the data.

Foraging speed experiments. For these experiments, new bees (not those that had completed the differential conditioning experiment) were used. During the training phase, each bee was allowed to forage freely on three training foraging speed flowers (as described above but without any test-squares, see Extended Data Fig. 7g) containing 30 µl of 30% sucrose solution, set 30 cm apart from one another. A bee was considered trained after it had completed at least three successful bouts of foraging.

During the test phase, three foraging speed flowers, displaying identical black smooth test-squares and offering 15 µl of 30% sucrose solution, were set 30 cm apart from one another in the arena (position 1). An individual bee was introduced to the arena and its foraging bout (recorded from the time it landed on the first flower until it landed on the third flower) was recorded with a Panasonic Lumix DMC-FZ38 camera. A large reward (100 µl of 30% sucrose solution) was offered to the bee at the end of the foraging bout to allow it to fill up and encourage it to return to the hive. Parts of the flowers with which the bees came into contact were cleaned with 20% ethanol to remove scent marks and set 30 cm apart from one another in a new location (position 2). The experiment was repeated with the same bee, but with flowers in position 2. For the third and fourth foraging bouts, the same bee was allowed to forage on three flowers, associated with black test strips overlain with a manufactured disordered grating, set at position 1 (third foraging bout) and position 2 (fourth foraging bout). For the fifth and sixth foraging bouts, the experiment was repeated using the same bee, but this time using flowers that displayed black test strips overlain with a manufactured perfect grating. This series of six foraging bouts, alternating between position and type of test-strips, was repeated using the same bee, with two new positions for the flowers (position 3 and 4). The entire procedure (twelve foraging bouts in total) was then repeated a minimum of four times to ensure that at least six complete foraging bouts on each flower type were recorded for each individual bee. This routine allowed us to control for the variability in foraging speed between foragers (as each bee performed the experiment on each type of flower) and any potential effect of the position of the flowers in the arena. Ten individuals were independently tested in total. The training phase and test phase were repeated twice, each time with ten new bumblebees; one of the repetitions alternated between smooth and manufactured disordered gratings associated with a yellow pigment, and the other alternated between smooth and manufactured disordered gratings associated with a blue pigment. The time taken for each bee to travel between each flower was extracted from the recordings using Wondershare Video Software. After examining the plots of residuals, a single-factor ANOVA and a post hoc Tukey's HSD test were conducted in RStudio (Version 0.99.902) to explore differences between artificial flower types.

Code availability. Code examples used in this study to plot the presented data are available in the Open Science Framework project, with the identifier https://osf.io/4tpp2.

Data availability. All data that support the findings of this study are available in the Open Science Framework project, with the identifier https://osf.io/4tpp2.

33. Yasin, S., Hasko, D. G. & Ahmed, H. Fabrication of <5 nm width lines in poly(methylmethacrylate) resist using a water:isopropyl alcohol developer and ultrasonically-assisted development. *Appl. Phys. Lett.* **78,** 2760–2762 (2001).
34. Williams, S. S. *et al.* High-resolution PFPE-based molding techniques for nanofabrication of high-pattern density, sub-20 nm features: a fundamental materials approach. *Nano Lett.* **10,** 1421–1428 (2010).
35. Dyer, A. G. & Chittka, L. Biological significance of distinguishing between similar colours in spectrally variable illumination: bumblebees (*Bombus terrestris*) as a case study. *J. Comp. Physiol. A Neuroethol. Sens. Neural Behav. Physiol.* **190,** 105–114 (2004).
36. Foster, J. J. *et al.* Bumblebees learn polarization patterns. *Curr. Biol.* **24,** 1415–1420 (2014).
37. Warton, D. I. & Hui, F. K. C. The arcsine is asinine: the analysis of proportions in ecology. *Ecology* **92,** 3–10 (2011).

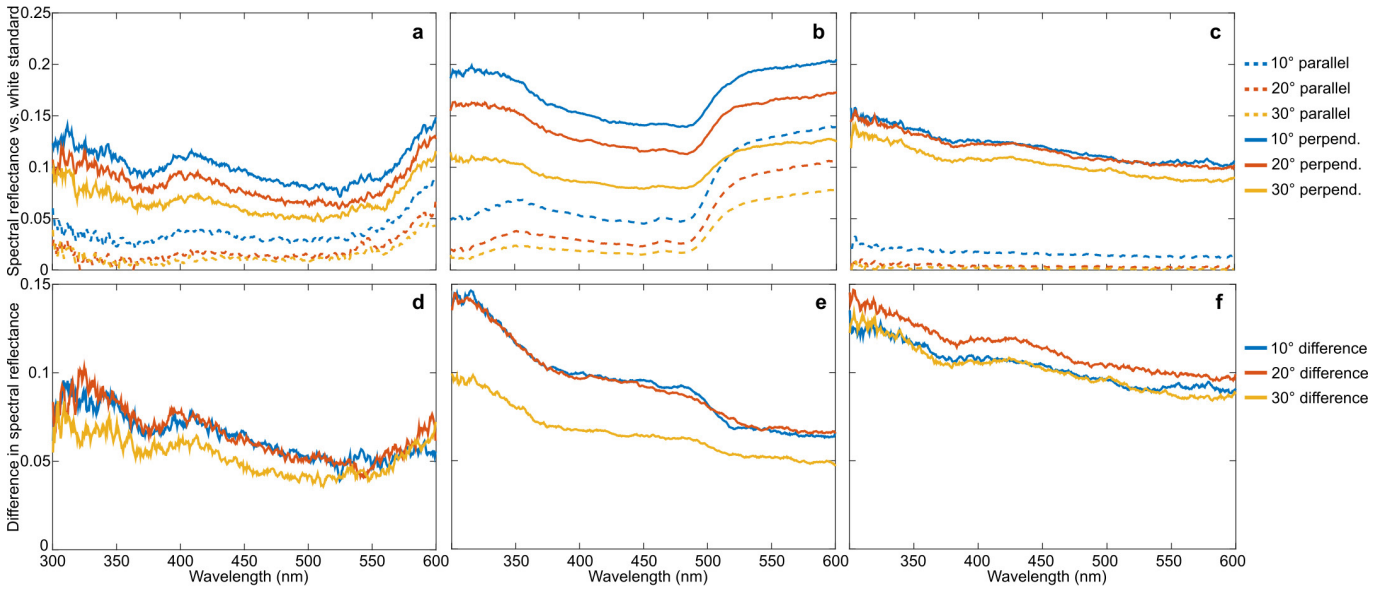

Extended Data Figure 1 | Spectral reflectance curves. a–**c**, Individual reflectance spectra of the three flowers in Fig. 2 are shown at scattering angles of 10°, 20° and 30°, recorded in parallel and perpendicular planes (with respect to the direction of surface striations), relative to the reflection of a white standard. **d**–**f**, Reflectance difference after subtracting parallel from perpendicular orientation measurements, revealing enhanced scattering for shorter wavelengths. **a**, **d**, *A. aestivalis* at negative angles; **b**, **e**, *O. stricta* reflectance reduced by a factor of ten to fit plot limits; **c**, **f**, *H. trionum* at negative angles.

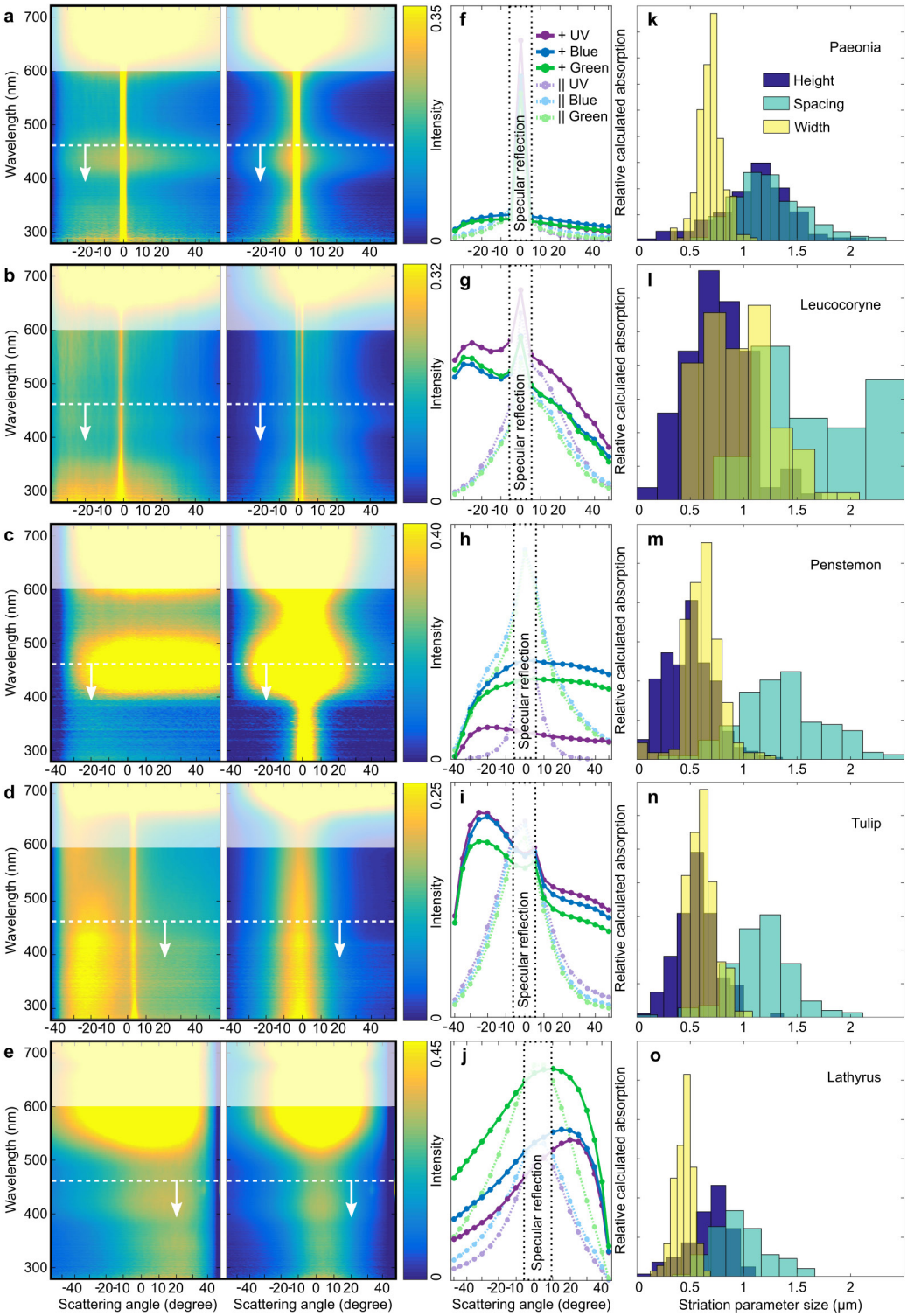

Extended Data Figure 2 | Optical response and anatomical parameters of petals with cuticular striations (*P. mascula, L. purpurea, P. barrettiae, Tulipa* 'Queen of the Night' and *L. aureus*). a–e, Scattering measurements from flowers with differing degrees of disorder; *P. mascula* (**a**), *L. purpurea* (**b**), *P. barrettiae* (**c**), *Tulipa* 'Queen of the Night' (**d**) and *L. aureus* (**e**). The images are two-dimensional plots showing the spectra of the scattered light in function of the sine-scale collection angle, relative to the location of the specular reflection (set to zero degrees). The intensity of the light is represented on a blue–yellow colour scale. The left column shows the angle distribution of the scattered light in the plane perpendicular to the striation direction, whereas in the right column the direction of the striations is parallel to the plane of collection. The angle of light incidence is 45° for all measurements. The colour scale in the scattering plots (normalized to a white diffuser standard) is kept constant for the same flower, but varies from flower to flower. To emphasize the blue halo, the spectral region between 600 and 700 nm (which is not perceived by the bees) is partially masked; horizontal dotted lines with downward arrows indicate the enhanced spectral region of the blue halo. **f–j**, Angle-dependent spectral response mediated on the three bee photoreceptors. Each of the points in the graph corresponds to an integral over the measured spectrum at the corresponding collection angle, after it has been weighted by the normalized sensitivity curves of the three types of photoreceptors in bee eyes, ultraviolet (in violet), blue (in blue) and green (in green). The spectra in the planes perpendicular and parallel to the striation direction are reported as darker and lighter colours, respectively. See Methods for additional details. **k–o**, Histograms of the measured striation parameters in terms of spacing and size (height and width), extracted from the TEM images, quantifying the amount of disorder.

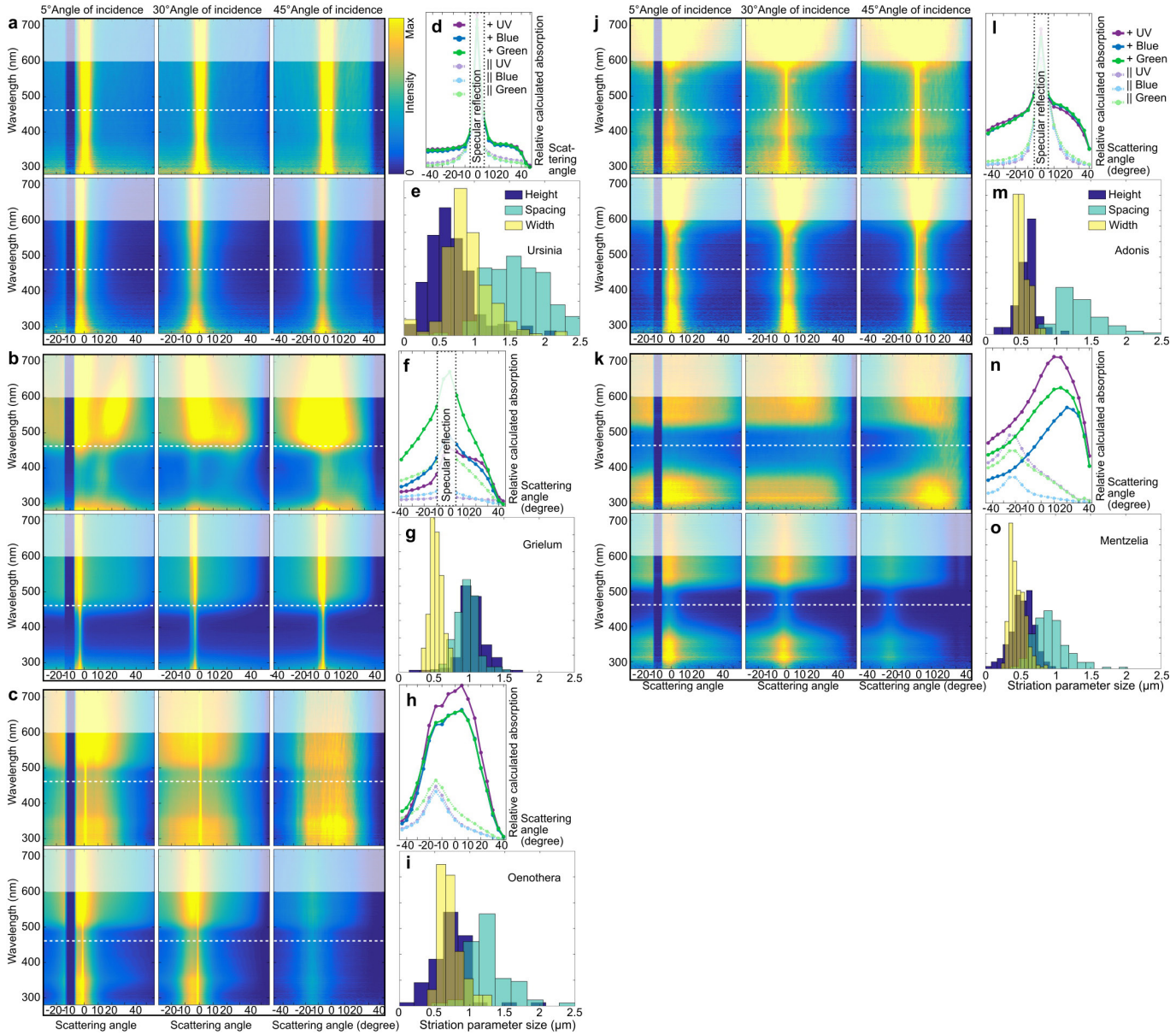

Extended Data Figure 3 | Optical response and anatomical parameters of petals with cuticular striations (*U. speciosa, G. humifusum, O. stricta, A. aestivalis and M. lindleyii*). **a**–**c**, **j**, **k**, Scattering measurements from flowers with differing degrees of disorder; *U. speciosa* (**a**), *G. humifusum* (**b**), *O. stricta* (**c**), *A. aestivalis* (**j**) and *M. lindleyii* (**k**). The images are two-dimensional plots showing the spectra of the scattered light in function of the collection angle, relative to the location of the specular reflection (set to zero degrees). The intensity of the light is represented on a blue–yellow colour scale. The upper row for each species shows the angular distribution of the scattered light in the plane perpendicular to the striation direction, whereas in the lower row the direction of the striations is parallel to the plane of collection for a range of angles. For each flower, three sets of measurements are shown for the angles of light incidence onto the petals as reported in the figure (5°, 30° and 45°). The colour scale in the scattering plots is kept constant for each pair of sample orientations, but its maximum value varies from flower to flower and between angles of incidence: **a**, 0.6, 0.6, 0.8; **b**, 1.6, 2.0, 2.0; **c**, 1.3, 1.5, 1.8; **j**, 0.35, 0.4, 0.55; **k**, 0.68, 0.8, 1.2 (all normalized to a white diffuser standard). To emphasize the blue halo, the spectral region between 600 and 700 nm (which is not perceived by the bees) is partially masked; horizontal dotted lines indicate the enhanced spectral region of the blue halo. **d**, **f**, **h**, **l**, **n**, The top plot on the right for each species reports the angle-dependent spectral response mediated by the three bee photoreceptors. Each of the points in the graph corresponds to an integral over the measured spectrum at the corresponding collection angle, after it has been weighted by the normalized sensitivity curves of the three types of photoreceptors in bee eyes, ultraviolet (in violet), blue (in blue) and green (in green). The spectra in the planes perpendicular and parallel to the striation direction are reported as darker and lighter colours, respectively. See Methods for additional details. **e**, **g**, **i**, **m**, **o**, Histograms of the measured striation parameters in terms of spacing and size (height and width), extracted from the TEM images, quantifying the amount of disorder.

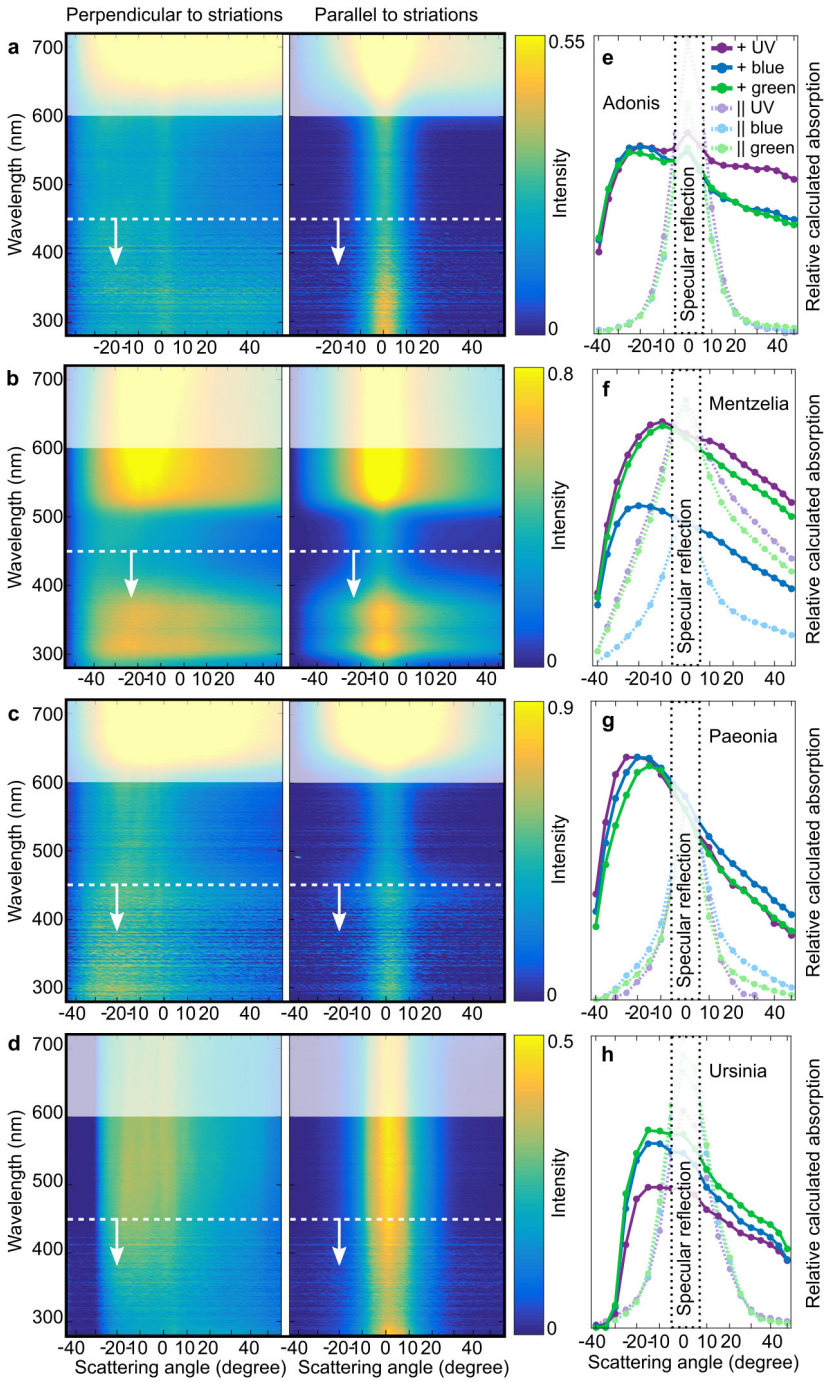

Extended Data Figure 4 | Repeated optical measurements of flowers. Additional scattering measurements for flowers in which the effect is particularly hard to identify from the single batch of measurements presented in Fig. 2 and Extended Data Figs 2, 3. Datasets were collected separately for different years to analyse the effect multiple times for the same species. Some of the measurements show the effect of the halo better than others; for consistency, the main text presents only a single dataset, in which all the flowers had been measured recently with the same experimental setup. This figure introduces samples from additional datasets, with minor differences (mainly in terms of the intensity of the lamp and the angular resolution) between the experimental setups. **a**–**d**, Scattering measurements from flowers with differing degrees of disorder; *A. aestivalis* (**a**), *M. lindleyii* (**b**), *P. mascula* (**c**) and *U. speciosa* (**d**). The images are two-dimensional plots showing the spectra of the scattered light in function of the sine-scale collection angle, relative to the location of the specular reflection (set to zero degrees). The left column shows the angle distribution of the scattered light in the plane perpendicular to the striation direction, whereas in the right column the direction of the striations is parallel to the plane of collection. The angle of light incidence is 45° for all measurements. The colour scale in the scattering plots is kept constant for the same flower, but it varies from flower to flower. To emphasize the blue halo, the spectral region between 600 and 700 nm (which is not perceived by the bees) is partially masked; horizontal dotted lines with downward arrows indicate the enhanced spectral region of the blue halo. **e**–**h**, Angle-dependent spectral response mediated on the three bee photoreceptors. See Methods for additional details.

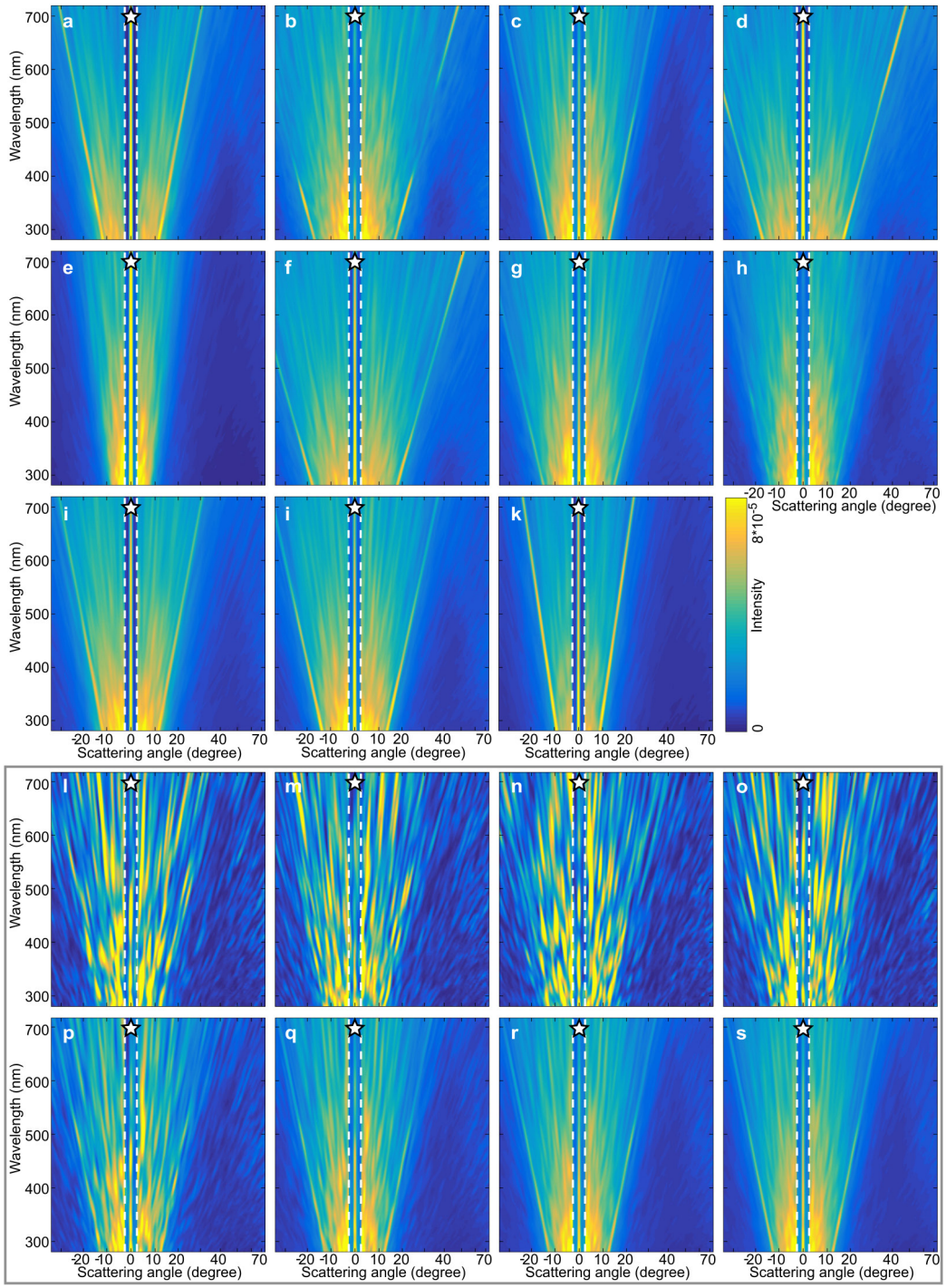

Extended Data Figure 5 | Simulated effect of disorder in cuticular striations for different flowers. FDTD simulation of the scattering responses of rectangular gratings with parameters and disorder according to the measured flower parameters of *A. aestivalis* (**a**), *G. humifusum* (**b**), *H. trionum* (**c**), *L. aureus* (**d**), *L. purpurea* (**e**), *M. lindleyii* (**f**), *O. stricta* (**g**), *P. mascula* (**h**), *P. barrettiae* (**i**), *Tulipa* 'Queen of the Night' (**j**) and *U. speciosa* (**k**). The intensity of the light is represented on a blue–yellow colour scale. The bands denoted by stars (**a**–**c**, **f**), containing the zero-order reflections, were reduced in intensity by a factor of three compared to the other regions of the graph. The additional graphs (**l**–**s**, grey box) demonstrate the process of averaging individual results to reveal the representative scattering pattern associated with the corresponding amount of disorder. These graphs contain the FDTD simulation results of rectangular gratings with dimensions equivalent to the *H. trionum* parameters, as in Fig. 3 (730 nm height, 730 nm width, 1,300 nm spacing; standard deviations: 0.27 height, 0.16 width and 0.29 spacing). **l**–**o**, Scattering plots of individual FDTD simulation results (as described in Methods). **p**, Average of scattering plots in **l**–**o**. The reduction in first-order interference and the appearance of a blue halo can be observed using a small sample number, but they become representative only when using averages of larger sample numbers, as in **q** (20×), **r** (40×) and **s** (60×). This observation also confirms that it is necessary to average a number of measurements taken at the same configuration or to illuminate a large area, in order to capture the colour-dependent scattering in a real flower petal with disorder. Depending on the size of the illuminated area, the measurement of a semi-disordered surface may have a similar appearance to the averages shown here, or appear randomly pixelated[17]. The minimum illuminated area required to observe representative distributions on flower petals is smaller than that required for the artificial samples, because natural striations vary slightly in their direction of propagation, whereas our artificial lines remained strictly parallel (providing less parameter variation for the same 2D area).

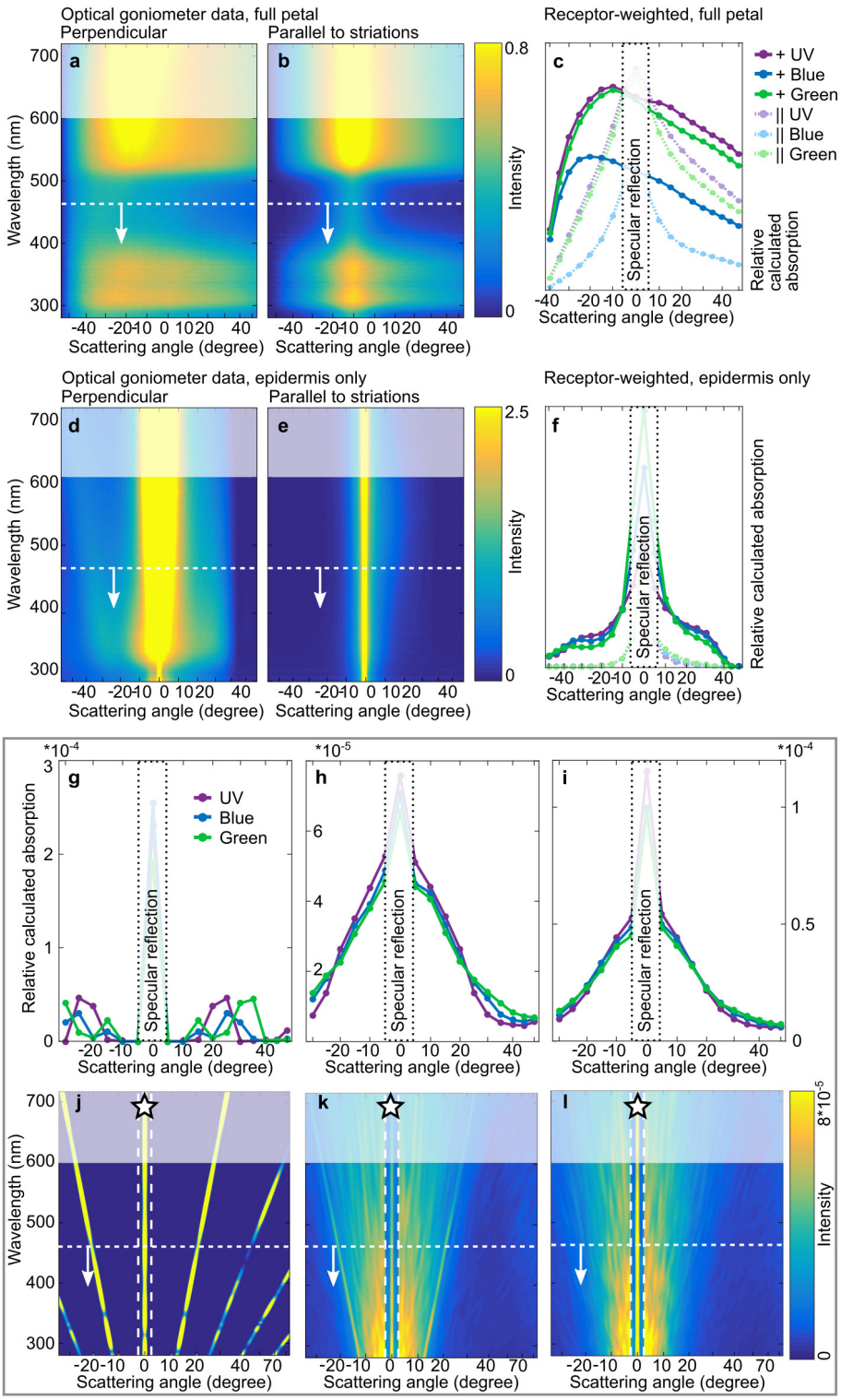

Extended Data Figure 6 | See next page for caption.

Extended Data Figure 6 | The effect of pigmentation on flower optical response. a–f, Optical measurements at 45° angle of incident light are presented for an *M. lindleyii* flower petal (**a**–**c**) and its peeled-off epidermal layer (**d**–**f**). For the entire petal (**a**, **b**), UV and yellow pigment colouration is visible at all angles and in both scanning directions (perpendicular and parallel to the direction of the striations). This produces high relative values for the UV receptor and green receptor, respectively (**c**). For colours corresponding to all three photoreceptors, more light is scattered perpendicular to the striations than parallel to them. At the same time, the overlapping optical signal of pigmentation makes it hard to recognize the colour trend of the surface-scattered light (the blue halo). When measuring the optical response of the striations on only the peeled-off epidermis, however, most pigments have been removed and the scattering collected perpendicularly to the striations (**d**) is caused by the structure itself. Almost no scattering is observed outside of the specular reflection when measuring parallel to the striation direction on peeled-off epidermis (**e**). In this case, the colouration of the halo becomes more apparent. The scattered light is enhanced in the low-wavelength (blue–UV) region and is most intense between −25° and +25° (**f**). **i–l**, To provide a qualitative comparison for the colouration effect observed on the peeled epidermis, we prepared a set of simulation results (using *H. trionum* parameters) in the same bee-receptor plot (grey box). Angle-dependent spectral response mediated on the three bee photoreceptors (**g**–**i**) in the simulations with *H. trionum*-derived parameters (**j**–**l**), with varying degrees of disorder (**g**, **j**, ordered; **h**, **k**, 1× natural disorder; **i**, **l**, 2× natural disorder). As a result of the subtlety of the halo colouration and the overlapping spectral sensitivity of bee photoreceptors, the relative intensity differences between receptor values are small and decrease with increasing disorder beyond those values found in actual flower species. To emphasize the blue halo in the scattering plots (**a**, **b**, **d**, **e**, **j**–**l**), the spectral region between 600 and 700 nm (which is not perceived by the bees) is partially masked; horizontal dotted lines with downward arrows indicate the enhanced spectral region of the blue halo.

Extended Data Figure 7 | Artificial flowers used in behavioural experiments, appearance of yellow and blue pigmented test-squares and examples of flowers with a blue halo effect visible to the human eye. a–d, The blue halo effect is best seen by the human eye on a dark pigmented background. *Ursinia calendulifolia* (**a**, **b**) and *H. trionum* (**c**, **d**) flowers present a striated epidermis at the base of their petals, which overlaps with a darkly pigmented zone. Anthocyanin pigment produces the dark purple colour and disordered striations produce the blue halo effect, visible at the base of the ray florets (**b**) or the proximal region of the petals (**d**). **e**, Schematic representation of artificial flower used in differential conditioning experiments (depicted with a yellow pigmented test-square) and photograph of a bee feeding on such a flower (with a black, perfectly iridescent test-square). Rewards or punishment are presented in the lid of the black Eppendorf tube. **f**, Yellow test-squares with a smooth surface (Sm) or overlain by a manufactured disordered structure (Di) are hardly discernible from one another, even if the observation angle varies. **g**, Schematic representation of artificial flower used in the foraging speed experiment (depicted with a yellow test-square) and photograph of a marked forager feeding on such a flower (with a black, perfectly iridescent test-square). **h**, Blue test-squares with a smooth surface or overlain by a manufactured disordered structure (as in **g**) appear identical to one another at some angles but at other angles they display distinct shades and intensities of blue. Image in **a**, **b** taken by H. Rice.

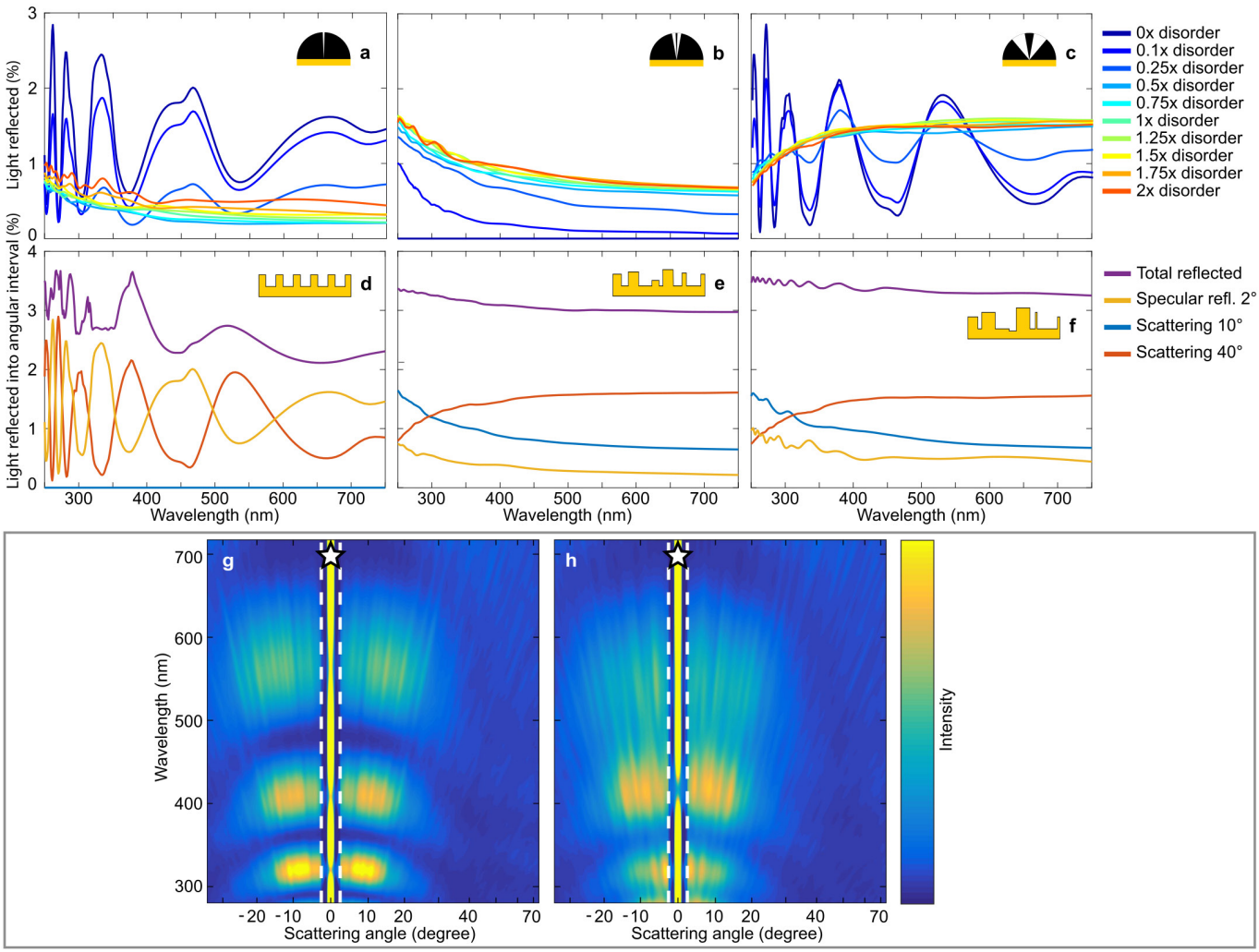

Extended Data Figure 8 | Angular components of the photonic effect of striations and role of height levels in disordered gratings. FDTD simulation spectra of rectangular gratings corresponding to *H. trionum* parameters, as in Fig. 3 (730 nm height, 730 nm width, 1,300 nm spacing). **a**, Specular reflection in the angular range from −2° to +2°, relative to the normal angle of incidence. **b**, Region of the blue halo between the specular reflection and the diffraction order peaks from −10° to +10°, excluding the region of specular reflection. This region was smaller than the full extent of the halo (which covers roughly between −20° and +20°) to avoid overlap with diffraction orders. **c**, Region spanning a large angular range from −40° to +40°, excluding the regions of **a** and **b**. This region contains the shorter wavelength parts of the first diffraction orders and the angles next to the high-intensity region of the blue halo. The change of the spectrum in the respective angular region is shown in **a**–**c**, with increasing disorder ranging from 0 (no disorder) through 1 (disorder corresponding to *H. trionum* parameters, standard deviations: 0.27 height, 0.16 width, 0.29 spacing) to 2, twice the standard deviation of natural disorder of *H. trionum*. **d**–**f**, Spectral response for the same three angular intervals as in **a**–**c**, together with the total amount of reflected light for one implementation of disorder each: no disorder (**d**), *H. trionum* levels of disorder (**e**), twice the disorder of *H. trionum* (**f**). The reduction in specular reflection can be observed in **a**, along with the reduction in thin film interference caused by the grating quasi-layer of intermediate refractive index. The fast rise of the blue halo for increasing disorder, and the stability of the effect for a wide range of disorder values, is shown in **b**. The quick decay of the first order diffraction components can be observed in **c**, along with the increased long-wavelength scattering response in this angular region. Note that the light reflected into this region is spread out over an angular range more than four times as large as the interval in **b**, reducing the scattered light intensity per viewing angle. The scattering response for incremental increases of striation disorder in **e** and **f** demonstrate the robustness of the blue halo effect with respect to the amount of disorder present in the striations. **g**, **h**, FDTD simulation results that reveal the role of height levels in disordered gratings. Simulation results are shown for rectangular gratings corresponding to the *H. trionum* parameters, as in Fig. 3 (730 nm height, 730 nm width, 1,300 nm spacing; standard deviations: 0.16 width and 0.29 spacing). **g**, Simulation without variation in height. The quasi-layer containing both air and grating teeth has an effective intermediate refractive index and results in thin film interference fringes. **h**, Simulation with one intermediate height level introduced at random in 40% of positions in the grating reduces thin-film interference and the colouration this causes. The artificial disordered gratings were manufactured by e-beam lithography from a thin film, which does not allow continuous variation in height.

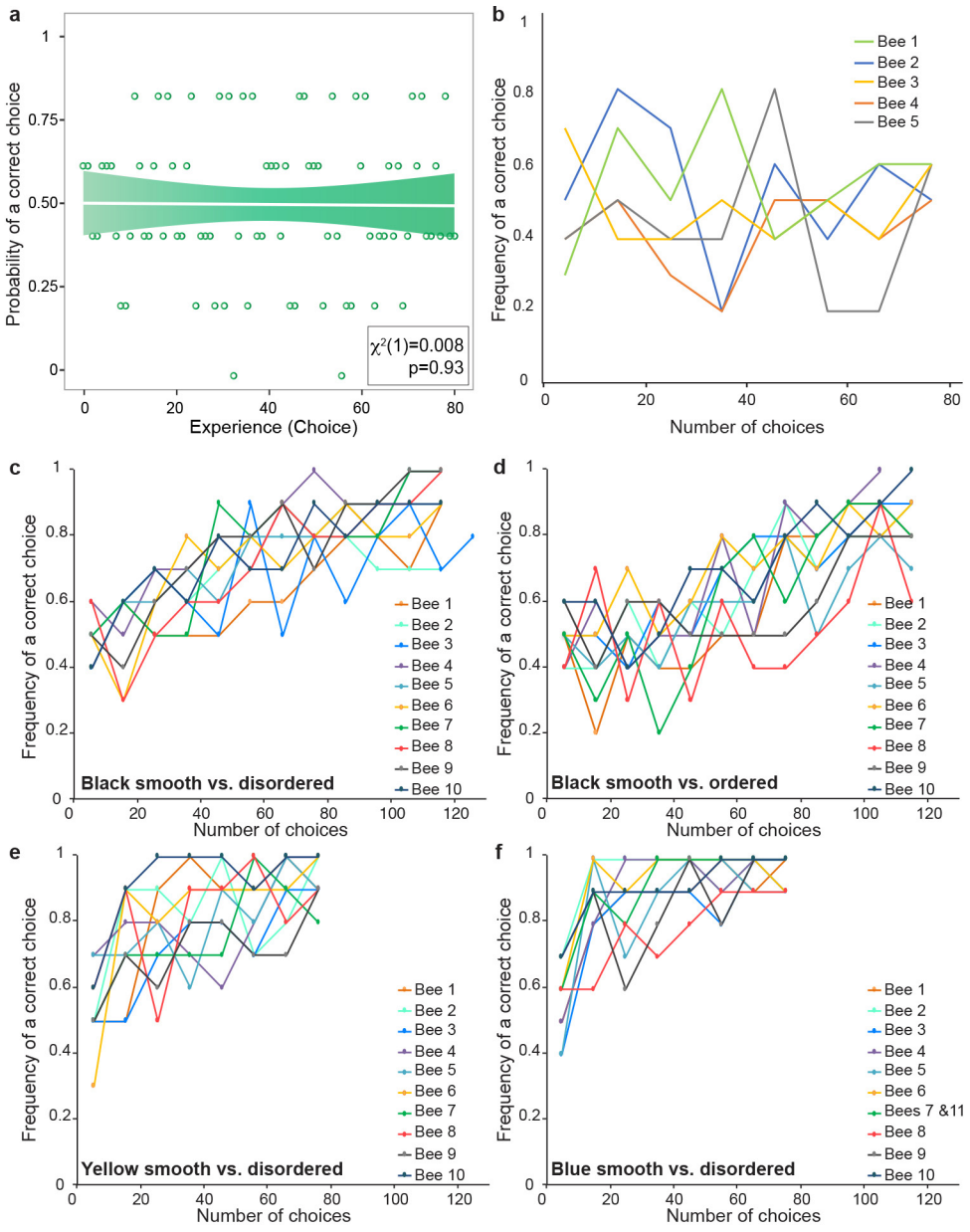

Extended Data Figure 9 | Behaviour of individual foragers during differential conditioning experiments. a, Learning curve of five bees choosing from among six black smooth artificial flowers (three punishing and three rewarding). Empty circles, mean proportion of bees making a correct choice, for each 80 successive choices. White curve, fitted binomial logistic model with green shading showing 95% confidence intervals on the fitted response. The χ^2 statistic and *P* value for the likelihood ratio test (assessing whether foragers can learn) are given at the bottom right of the panel. **b**, As in **a**, but showing the learning curves of each individual. The frequency of correct choice (rewarding flower) is calculated for every ten visits. None of the five foragers used in this experiment successfully managed to identify the rewarding flowers accurately even after 80 visits. **c**, Learning curve of ten individual bees choosing between black smooth and black disordered artificial flowers, as in Fig. 4b. The frequency of correct choice (rewarding flower) is calculated for every ten visits. **d**, As in **c**, but with bees choosing between black smooth and black ordered artificial flowers, as in Fig. 4c. **e**, As in **c**, but with ten bees choosing between yellow smooth and yellow disordered artificial flowers, as in Fig. 4d. **f**, As in **c**, but with 11 bees choosing between blue smooth and blue disordered artificial flowers, as in Fig. 4e.

Extended Data Table 1 | Disorder in cuticular striations for flower species

Species	Height μm	σ_H μm	Width μm	σ_W μm	Spacing μm	σ_D μm	Number of striations analysed
Adonis aestivalis	0.59	0.15	0.52	0.09	1.4	0.39	72
Grielum humifusum	1	0.20	0.53	0.09	0.97	0.16	111
Hibiscus trionum	0.73	0.27	0.73	0.16	1.3	0.29	74
Leucocoryne purpurea	0.74	0.29	0.96	0.31	2.1	0.86	141
Lathyrus aureus	0.67	0.20	0.44	0.09	0.98	0.25	118
Mentzelia lindleyii	0.53	0.17	0.45	0.11	0.92	0.24	323
Oenothera stricta	0.72	0.23	0.62	0.16	1.1	0.3	195
Paeonia mascula	1.1	0.34	0.64	0.12	1.2	0.34	270
Penstemon barrettiae	0.48	0.20	0.66	0.15	1.4	0.42	343
Tulipa 'Queen of the night'	0.55	0.18	0.61	0.12	1.2	0.3	150
Ursinia speciosa	0.75	0.22	0.88	0.19	1.6	0.4	319

The table reports the average value and standard deviation in μm of the dimensions (height and width) and the distances between striation minima (spacing) for the striations of different species, obtained from TEM images. See Extended Data Figs 2 and 3 for details of the parameters. The last column gives the number of unique striation cross-sections analysed for each species.

nature research

Corresponding author(s): Glover

☐ Initial submission ☐ Revised version ☒ Final submission

Life Sciences Reporting Summary

Nature Research wishes to improve the reproducibility of the work that we publish. This form is intended for publication with all accepted life science papers and provides structure for consistency and transparency in reporting. Every life science submission will use this form; some list items might not apply to an individual manuscript, but all fields must be completed for clarity.

For further information on the points included in this form, see Reporting Life Sciences Research. For further information on Nature Research policies, including our data availability policy, see Authors & Referees and the Editorial Policy Checklist.

Experimental design

1. Sample size

Describe how sample size was determined.

Sample size for bee experiments was determined using standard sample sizes from previous studies.

2. Data exclusions

Describe any data exclusions.

No data were excluded from the analyses.

3. Replication

Describe whether the experimental findings were reliably reproduced.

All floral measurements were repeated multiple times over a six year window, with different individual plants grown in a variety of conditions. While the quality of data varied, the essential patterns were reproducible.

4. Randomization

Describe how samples/organisms/participants were allocated into experimental groups.

n/a

5. Blinding

Describe whether the investigators were blinded to group allocation during data collection and/or analysis.

n/a

Note: all studies involving animals and/or human research participants must disclose whether blinding and randomization were used.

6. Statistical parameters

For all figures and tables that use statistical methods, confirm that the following items are present in relevant figure legends (or in the Methods section if additional space is needed).

n/a	Confirmed	
☐	☒	The exact sample size (*n*) for each experimental group/condition, given as a discrete number and unit of measurement (animals, litters, cultures, etc.)
☐	☒	A description of how samples were collected, noting whether measurements were taken from distinct samples or whether the same sample was measured repeatedly
☐	☒	A statement indicating how many times each experiment was replicated
☐	☒	The statistical test(s) used and whether they are one- or two-sided (note: only common tests should be described solely by name; more complex techniques should be described in the Methods section)
☐	☒	A description of any assumptions or corrections, such as an adjustment for multiple comparisons
☐	☒	The test results (e.g. *P* values) given as exact values whenever possible and with confidence intervals noted
☐	☒	A clear description of statistics including central tendency (e.g. median, mean) and variation (e.g. standard deviation, interquartile range)
☐	☒	Clearly defined error bars

See the web collection on statistics for biologists for further resources and guidance.

Software

Policy information about availability of computer code

7. Software

Describe the software used to analyze the data in this study.	Statistical analyses in R. Lumerical software for FDTD.

For manuscripts utilizing custom algorithms or software that are central to the paper but not yet described in the published literature, software must be made available to editors and reviewers upon request. We strongly encourage code deposition in a community repository (e.g. GitHub). *Nature Methods* guidance for providing algorithms and software for publication provides further information on this topic.

Materials and reagents

Policy information about availability of materials

8. Materials availability

Indicate whether there are restrictions on availability of unique materials or if these materials are only available for distribution by a for-profit company.	No restrictions.

9. Antibodies

Describe the antibodies used and how they were validated for use in the system under study (i.e. assay and species).	not applicable

10. Eukaryotic cell lines

a. State the source of each eukaryotic cell line used.	No cell lines used.
b. Describe the method of cell line authentication used.	*Describe the authentication procedures for each cell line used OR declare that none of the cell lines used have been authenticated OR state that no eukaryotic cell lines were used.*
c. Report whether the cell lines were tested for mycoplasma contamination.	*Confirm that all cell lines tested negative for mycoplasma contamination OR describe the results of the testing for mycoplasma contamination OR declare that the cell lines were not tested for mycoplasma contamination OR state that no eukaryotic cell lines were used.*
d. If any of the cell lines used are listed in the database of commonly misidentified cell lines maintained by ICLAC, provide a scientific rationale for their use.	*Provide a rationale for the use of commonly misidentified cell lines OR state that no commonly misidentified cell lines were used.*

Animals and human research participants

Policy information about studies involving animals; when reporting animal research, follow the ARRIVE guidelines

11. Description of research animals

Provide details on animals and/or animal-derived materials used in the study.	Not applicable.

Policy information about studies involving human research participants

12. Description of human research participants

Describe the covariate-relevant population characteristics of the human research participants.	Not applicable.